# Atypical developmental remodeling of dopamine neurons involves AKT-GSK3β signaling and glia activity

**Authors:**

Xiaofan Zhang[1], Wei Chen[1], Yayu Wang[1], Xun Tu[2], Xiangyu Zhang[1], Ronald L. Davis[3], Lily Yeh Jan[1], and Yuh Nung Jan[1,4,*]

**Affiliations:**

[1]Department of Physiology and Howard Hughes Medical Institute, University of California at San Francisco; San Francisco, CA 94158, USA.

[2]Division of Neurobiology, Department of Molecular and Cell Biology, Helen Wills Neuroscience Institute, Howard Hughes Medical Institute, University of California, Berkeley, CA 94720, USA

[3]Department of Neuroscience, UF Scripps Institute for Biomedical Research, Jupiter, FL 33458, USA

[4]Lead contact

*Correspondence: yuhnung.jan@ucsf.edu

**Summary**

Neuronal remodeling is essential for sculpting neural circuits, and its disruption has been implicated in neurodevelopmental and neuropsychiatric disorders. Yet the molecular and cellular diversity of remodeling across neuron types remains incompletely understood. Here, we uncover a distinct remodeling mode in a subtype of *Drosophila* dopamine neurons (DANs) critical for learning, memory, sleep, and locomotion. Unlike the stereotypical pruning-then-regrowth paradigm, these DANs undergo a transient axon overgrowth followed by selective pruning during metamorphosis. Remarkably, DAN axon pruning proceeds independently of canonical ecdysone signaling and instead involves neuron-intrinsic AKT-GSK3β signaling and extrinsic glial activity. Disruption of AKT-GSK3β signaling alters microtubule stability and impairs glial recruitment and clearance of axonal debris. Notably, the role of AKT-GSK3β is cell-type specific,

underscoring mechanistic diversity in remodeling programs. These findings reveal an unexpected overgrowth-then-pruning developmental trajectory, establishing DANs as a powerful model to uncover the mechanisms underlying neuronal remodeling, circuit maturation, and neurodegeneration.

## Introduction

Neuronal remodeling is a fundamental process that shapes the architecture and function of the nervous system during development and in response to experience[1–4]. Disruption of this process may contribute to a range of neurodevelopmental and neuropsychiatric disorders, including autism spectrum disorder and schizophrenia[3–7]. Growing evidence suggests that developmental neuronal remodeling and age-related neurodegeneration may share conserved molecular mechanisms, raising the possibility that similar pathways might govern neuronal degeneration across life stages[1,8,9].

The fruit fly *Drosophila melanogaster* has long served as a powerful model for investigating the cellular and molecular basis of neuronal remodeling. A well-characterized paradigm of developmental neuronal remodeling involves the pruning of larval-stage neurites followed by regrowth to establish adult-specific circuits during *Drosophila* metamorphosis. This stereotyped pruning-then-regrowth remodeling paradigm is exemplified in many neuron types across the central nervous system (CNS) and peripheral nervous system (PNS), including cholinergic Mushroom Body (MB) neurons, GABAergic anterior paired lateral (APL) neurons, and olfactory projection neurons (PNs) in the CNS, and dendritic arborization (da) neurons in the PNS[10–14]. Whether dopamine neurons (DANs) undergo a similar remodeling trajectory was unknown.

Neuronal remodeling is driven by a combination of intrinsic and extrinsic mechanisms. The steroid hormone ecdysone functions as an essential regulator of this process across diverse neuron types that undergo pruning-then-regrowth remodeling[10–15]. Ecdysone exerts its effects through cell-autonomously expressed ecdysone receptors and downstream pathways involving caspase signaling and the ubiquitin-proteasome system (UPS)[10,13–22]. However, whether ecdysone signaling universally governs neuronal remodeling across neuron types remains largely unknown.

Pruning of neurites during neuronal remodeling typically occurs through local degeneration, followed by debris clearance mediated by extrinsic non-neuronal cells. In the CNS, glial cells engulf and eliminate degenerating neurites from MB neurons and PNs[13,23,24]. In the PNS, epidermal cells function as primary phagocytes that remove dendritic debris from da neurons[25]. Whether DANs engage in similar remodeling dynamics or rely on comparable neuron–glia interactions during development remains an open question.

Here, we identify a previously unrecognized mode of neuronal remodeling in *Drosophila* DANs. In contrast to the stereotypical pruning-then-regrowth remodeling paradigm, DANs exhibit an atypical overgrowth-then-pruning remodeling trajectory, characterized by the transient overextension of a new axon branch from an established circuit during a narrow developmental window, which is subsequently selectively pruned to establish adult-stage circuitry. Remarkably, this pruning process occurs independently of canonical ecdysone signaling, caspase activity, and the ubiquitin-proteasome system. Instead, we identify the AKT-GSK3β signaling pathway as a critical cell-intrinsic regulator of this process. We further show that DAN axon pruning proceeds through a local degeneration mechanism that involves an interplay between AKT-GSK3β signaling, microtubule cytoskeleton, and glial activities. Given the essential roles of AKT-GSK3β signaling and glial activity in DAN degeneration in Parkinson's disease (PD), our findings raise the possibility that shared principles may link DAN pruning with disease-associated neurodegenerative processes[1,8,9,26–29].

## Results:

### Atypical developmental remodeling of dopamine neurons in *Drosophila*

To investigate whether dopamine neurons (DANs) undergo developmental remodeling, we focused on the PPL1 (protocerebral posterior lateral 1) cluster of DANs in the central brain of *Drosophila melanogaster* (fruit fly). The PPL1 cluster consists of approximately 12 DANs per hemisphere, which can be divided into five distinct subtypes with stereotyped innervation patterns across different compartments of the Mushroom Body (MB) axons[30,31] (Figure S1A and S1B). PPL1 DANs are essential for learning and memory, forgetting, sleep, and locomotion, thus sharing several functional and

88 mechanistic similarities with DANs in the substantia nigra pars compacta (SNc) of
89 mammals[32–35]. Moreover, PPL1 DANs represent the only DAN subset that consistently
90 undergoes neurodegeneration across multiple *Drosophila* Parkinson's disease (PD)
91 models[36–38], making them an excellent system for investigating the mechanisms
92 underlying DAN development in both health and disease.

93 We used the TH-D'-Gal4 driver to label PPL1 DANs[32] and trace their development
94 across various stages. While TH-D'-Gal4 labels approximately 12 DANs that project to
95 the vertical lobe, junction, and heel regions of the MB in adult flies, we found that at the
96 third instar larval stage, it labels only 3 DAN cell bodies, whose axons predominantly
97 innervate the heel region (corresponding to the MP1 or PPL1γ1pedc region, hereafter
98 referred to as MP1) (Figure S1B). This observation aligns with previous reports
99 indicating that TH-D'-Gal4 primarily labels MP1 DANs at the third instar larval stage[39].

100 During metamorphosis, the MB lobes undergo dramatic remodeling: their larval-stage-
101 specific vertical and horizontal lobes are pruned within 18 hours after puparium
102 formation (APF), followed by regrowth of the horizontal lobe beginning around 24 hr
103 APF to establish adult-specific connectivity[12,19]. Notably, a pair of GABAergic APL
104 neurons, which innervate the MB, including the MP1 region, exhibit a comparable
105 remodeling pattern involving axon pruning and subsequent regrowth[14]. Given that both
106 APL neurons and MP1 DANs innervate the MB, and that both APL neurons and MB
107 itself remodel within a similar time frame[12,14,19], we asked whether MP1 DANs follow a
108 comparable remodeling trajectory.

109 Unexpectedly, we observed an overgrowth of DAN axons from the densely innervated
110 MP1 branch into the MB's junction region (also known as the MV1 region) between 12
111 hr and 18 hr APF (Figure 1A and 1D-1E). However, this newly extended branch is
112 transient and is progressively pruned after 24 hr APF (Figure 1A and 1F-1H). Further
113 analysis (detailed below, Figure 2) confirmed that this structure represents an
114 overextension of axons from a single pair of MP1 DANs into the degenerating MB MV1
115 region (Figure 3A-3B and S3A-S3B), which we designated as the MP1o branch.
116 Notably, the MP1o branch was not observed prior to 6 hr APF (Figure 1A-1C),

117 suggesting that it emerges between 6 hr and 12 hr APF, and it is largely pruned by 30–
118 36 hr APF (Figure 1A, 1G-1H).

119 Quantification of the relative area occupied by MP1/MP1o branches revealed a
120 significant increase at 12, 18, and 24 hr APF compared to 0 hr APF (Figure 1I). We
121 further validated these findings using the split-Gal4 driver MB320C, which specifically
122 labels MP1 DANs in adult flies[40], and found that it recapitulated the overgrowth
123 phenotype at 18 hr APF (Figure S1C).

124 Together, these results demonstrate that DANs undergo developmental remodeling
125 during metamorphosis. Whereas previous studies of developmental remodeling have
126 documented a stereotypical pruning-then-regrowth pattern for MB neurons, PNs, APL
127 neurons, and da neurons[10–14], DANs exhibit an atypical overgrowth-then-pruning
128 remodeling pattern characterized by an initial overgrowth phase followed by pruning
129 (Figure 1J).

130 **A single pair of DANs undergoes atypical remodeling during metamorphosis**

131 At both 0 and 18 hr APF, TH-D'-Gal4 labels approximately three cell bodies within the
132 PPL1 cluster (Figure S2A-S2B, left panels). Immunostaining with anti-tyrosine
133 hydroxylase (TH) antibodies confirmed that all three somas were TH-positive, indicating
134 they are DANs (Figure S2A-S2B, middle and right panels). We thus asked whether the
135 MP1 branch and the overextended MP1o branch originate from the same neuron or
136 from distinct neurons among the three labeled DANs.

137 To address this, we used photoactivatable GFP (C3PA-GFP)[41] to examine GFP diffusion
138 between the MP1 and MP1o branches. We reasoned that if these two branches arose
139 from the same neuron, localized photoactivation in one branch would lead to GFP
140 diffusion into the other. Consistent with this hypothesis, photoactivation of the MP1
141 branch resulted in rapid GFP diffusion into the MP1o branch at both 18 and 24 hr APF
142 (Figure 2A, 2D). In contrast, although we occasionally observed branch-like structures
143 in the MV1 region resembling the MP1o branch at 0 hr APF, no GFP diffusion was
144 detected between the MP1 branch and these structures (Figure 2A), confirming that the
145 MP1o branch is not present at this earlier stage.

146 To further confirm that the MP1 and MP1o branches originate from a single DAN, we
147 tracked GFP diffusion from axons in the MP1 branch back to their somas. Time-lapse
148 imaging revealed that only one of the three DAN somas gradually accumulated GFP
149 signal at 18 hr APF (Figure 2B, 2E), indicating it is directly connected to the MP1/MP1o
150 branches. The remaining two DAN somas retained baseline levels of C3PA-GFP signal
151 (Figure 2B, 2E, soma 1 and 2).

152 Similarly, the split-Gal4 driver MB320C labeled three somas at 18 hr APF (Figure S1C),
153 consistent with TH-D'-Gal4 labeling. However, MB320C progressively lost labeling of the
154 two non-MP1 DAN somas and ultimately labeled only the single MP1 DAN in the adult
155 brain (Figure S1C, 48 hr APF and adult). The fate and function of the two non-MP1
156 DANs remain unknown and require further investigation. Together, these findings
157 demonstrate that a single pair of MP1 DANs (one per brain hemisphere) undergoes
158 atypical developmental remodeling during *Drosophila* metamorphosis.

159 **The MP1 DAN in each hemisphere innervates both hemispheres during**
160 **development and in adulthood**

161 Surprisingly, localized photoactivation of the MP1 branch in a single hemisphere at 18
162 hr APF led to GFP diffusion not only within the targeted hemisphere, but also into the
163 soma and axons of the MP1 DAN in the contralateral hemisphere (Figure 2B, S2C).
164 This indicates that each MP1 DAN projects its axons not only ipsilaterally within the
165 hemisphere but also contralaterally across the midline so that both hemispheres receive
166 its innervation during development.

167 To confirm this observation, we photoactivated the MP1 DAN soma in one hemisphere
168 and observed GFP diffusion into the MP1/MP1o branches in both hemispheres (Figure
169 2C, 2F), further supporting the bilateral projection pattern.

170 We next asked whether this bilateral projection pattern persists into adulthood. Using
171 MB320C-Gal4-driven C3PA-GFP expression in adult flies, photoactivation of a single
172 MP1 DAN soma again resulted in GFP diffusion into MP1 branches in both hemispheres
173 (Figure S2E-S2F), demonstrating that this bilateral connectivity is maintained beyond
174 development. Given the established roles of MP1 DANs in memory formation and

175 forgetting[40,42–45], the bilateral innervation pattern may function to coordinate
176 dopaminergic modulation across hemispheres during these cognitive processes.

177 **The MP1o branch includes axons presynaptic to the MB**

178 During developmental remodeling of MB γ neurons, the larval stage γ neuron axon
179 lobes are pruned, whereas axons in the junction (MV1) and heel/peduncle (MP1)
180 regions are left largely intact[12,19] (Figure 6E). The mechanisms that limit pruning to
181 specific regions remain unknown. Subsequently, the adult-specific γ lobe regrows from
182 the MV1/junction region[46].

183 Interestingly, we found that the MP1o branch specifically targets the MV1 region of the
184 MB, as shown by both anti-FasII and anti-nc82 (a presynaptic marker) staining at 12
185 and 18 hr APF (Figure 3A-3C and S3A-S3B). In fact, the MP1o branch appeared to be
186 attracted to the MV1 region, with its distal part confined near the MV1 boundary (Figure
187 3A, dashed line). This innervation pattern was further confirmed in single confocal
188 sections (Figure 3B). 3D reconstruction of the MP1/MP1o branch and MB axons reveals
189 that the MP1o branch broadly innervates the entire MB MV1 region (Movie 1). Thus, the
190 MP1o branch represents an overextended branch of MP1 DANs that transiently
191 innervates the degenerating but unpruned MB MV1 region during active MB remodeling.

192 To test whether the MP1o branch forms synapses with the MB, we used GFP
193 reconstitution across synaptic partners (GRASP)[47] and observed reconstituted GFP
194 signal in the MV1 region at 18 and 24 hr APF (Figure 3D, S3C). This finding suggests
195 potential synaptic contacts between the MP1o branch and MB. In addition, we detected
196 Bruchpilot:GFP (Brp-GFP), a presynaptic active zone marker[48], in the MP1o branch at
197 18 and 24 hr APF (Figure 3E, S3D), indicating that the MP1o branch possesses
198 presynaptic machinery. Together, these results suggest that the MP1o branch is likely
199 functionally integrated with the MB.

200 **Local degeneration and glial involvement in MP1 DAN axon pruning**

201 Axon degeneration is a hallmark of many neurodegenerative disorders. In PD, DAN
202 axon degeneration often precedes soma loss, following a “dying-back” pattern in which
203 axons degenerate progressively from distal synaptic terminals toward the cell body[49–51].

204 It thus appears that preventing or delaying axon degeneration could be a viable strategy
205 to slow disease progression[1,52,53].

206 Axon pruning of MB γ neurons and dendrite pruning of peripheral da neurons have been
207 shown to occur via local degeneration[23–25,54,55]. To determine whether pruning of the
208 MP1o branch of MP1 DANs also involves local degeneration, we examined key
209 hallmarks of this process: axons fragmentation and phagocyte-mediated clearance of
210 neuronal debris[1,2,19,55].

211 Unlike the long axonal or dendritic tracts of MB γ neurons or class IV da (daIV)
212 neurons[19,25], the MP1o branch is short with densely intertwined axons (Figure 3A-3B),
213 making it challenging to observe stereotypical fragmentation patterns. Nevertheless, we
214 observed signs of disconnected axonal fragments at the distal end of the MP1o branch
215 at 24-36 hr APF (Figure 1F-1H), suggesting that local degeneration may take place in
216 the MP1o branch. In support of this notion, our data using *shi*$^{ts}$-mediated inhibition of
217 glial cells indicate that axon fragmentation occurs during pruning of the MP1o branch
218 (Figure 4F, 4H).

219 Another hallmark of local degeneration is the involvement of phagocytes in engulfing
220 and clearing fragmented neuronal debris. For example, glial cells have been shown to
221 mediate MB γ neuron axon pruning by engulfing fragmented axons[23,24]. We asked
222 whether glial cells similarly participate in pruning of the MP1o branch. To address this
223 question, we first examined whether glial cells accumulate in the MP1/MP1o region
224 during pruning, which would indicate their involvement. Using an anti-Repo antibody to
225 label glial nuclei, we observed a significant increase in the number of glial cells in the
226 MP1/MP1o branches at 24 and 30 hr APF compared to 18 hr APF (Figure 4A-4B).

227 Local degeneration involves active infiltration of glial processes into the degenerating
228 neuropil[23,24,56]. To investigate this possible scenario, we used membrane-bound RFP
229 driven by the glial-specific repo promoter (Red-Repo) to visualize glial processes in the
230 MP1/MP1o region. In line with the observed increase in glial cell number, we detected
231 enhanced infiltration of glial processes into the MP1/MP1o region at 24 and 30 hr APF
232 relative to 18 hr APF (Figure 4C-4D).

233 Glial processes in the MP1/MP1o region exhibited punctate morphologies (Figure 4C),
234 reminiscent of the “lumps” formed during the engulfment and degradation of
235 degenerating γ neuron axons[24,54]. This observation raised the possibility of active glial
236 engulfment of degenerating DAN axons, likely involving the endosomal-lysosomal
237 pathway[23,24]. To test this possibility, we labeled endosomal-lysosomal compartments
238 using LysoTracker and simultaneously visualized axons in the MP1/MP1o branches and
239 glial processes. At 24 hr APF, we observed considerable number of LysoTracker-
240 positive puncta in the MP1o region that colocalized with puncta of glial processes as
241 well as axons in the MP1/MP1o branches (Figure 4E and S4A-S4B). These findings
242 suggest active glial engulfment during MP1o pruning.

243 To further study the role of glial cells in MP1o pruning, we blocked glial endocytic activity
244 by targeted expression of a temperature-sensitive *shibire* (*shi*$^{ts}$) construct in glial cells
245 (Figure 4F). *Shibire* encodes Dynamin, a GTPase essential for endocytosis,
246 phagocytosis, and membrane trafficking[57]. *Shi*$^{ts}$ functions as a dominant-negative
247 variant at restrictive temperatures (>29°C), thereby inhibiting endocytosis and other
248 membrane-associated processes[58]. Previous studies have shown that *shi*$^{ts}$ expression
249 in glia impairs glial process infiltration and delays MB γ lobe degeneration during
250 developmental pruning[24].

251 When we shifted pupae raised at the permissive temperature (23°C) to the restrictive
252 temperature (29°C) from ~7 hr to 24 hr APF, we observed a significant reduction in the
253 infiltration of glial processes into the MP1/MP1o region in the *shi*$^{ts}$ group compared to
254 control (Figure 4F-4G). Additionally, we detected an increase in axon debris, appearing
255 as punctate structures within the MP1o region in the *shi*$^{ts}$ group relative to the control
256 (Figure 4F and 4H), suggestive of impaired glia-mediated engulfment or degradation
257 process. Together, these results demonstrate that pruning of MP1 DAN axons involves
258 local degeneration and glial activity.

259 **Canonical ecdysone signaling is dispensable for MP1 DAN axon pruning**

260 We next sought to investigate the cell-autonomous mechanisms underlying pruning of
261 the MP1o branch. Ecdysone signaling is well-established as a key regulator of
262 developmental pruning in various neuron types[10,12–15]. To test whether ecdysone

263 signaling could similarly mediate DAN axon pruning, we expressed a dominant-negative
264 form of the ecdysone receptor isoform B1 (EcR-B1-DN) specifically in MP1 DANs using
265 MB320C-Gal4 and examined the fate of the MP1o branch. If ecdysone signaling were
266 required for pruning, we would expect the MP1o branch to persist into adulthood upon
267 EcR-B1-DN expression.

268 To our surprise, expression of EcR-B1-DN did not impair MP1o pruning, as axons in the
269 MP1o branch were not detected in adult flies (Figure 5A). As a positive control validating
270 the functionality of the construct, expression of EcR-B1-DN in MB γ neurons robustly
271 blocked γ lobe pruning (Figure S5A). Moreover, expression of a DN form of the EcR-A
272 isoform (EcR-A-DN) did not disrupt MP1o pruning (Figure 5B). These findings made us
273 wonder whether MP1 DANs express significant levels of ecdysone receptors.

274 EcR-B1 or EcR-A proteins are known to be expressed in MB γ neurons, da neurons,
275 and APL neurons at the onset of metamorphosis, where they play essential roles in
276 developmental remodeling[10,12,14]. However, using antibody staining, we did not detect
277 EcR-B1 or EcR-A protein expression above background levels in MP1 DAN cell bodies
278 at 0, 18, or 24 hr APF (Figure 5C-5D). In contrast, robust EcR-B1 expression was
279 observed in other brain regions (Figure S5B), confirming the reliability of our antibody
280 staining. Although we cannot exclude low-level expression below detection thresholds,
281 the absence of detectable EcR proteins in MP1 DANs is consistent with our genetic
282 data indicating that EcR signaling is not required for MP1o pruning.

283 Together, these findings indicate that canonical ecdysone signaling is dispensable for
284 pruning of the MP1o branch. While most neurons may rely on an ecdysone-dependent
285 remodeling program, MP1 DANs appear to undergo axon pruning through an ecdysone-
286 independent mechanism.

287 **Genetic screen reveals that AKT-GSK3β signaling is involved in MP1 DAN axon**
288 **pruning**

289 Although caspase activity and the UPS have been shown to be essential for
290 developmental remodeling[17–19,21], we found that MP1o pruning proceeds normally
291 despite perturbations to these pathways. Specifically, expression of a dominant-

292 negative form of the initiator caspase Dronc (Dronc-DN), as well as overexpression of
293 the caspase inhibitors p35 or DIAP1 – manipulations known to block dendrite pruning in
294 da neurons[17] – did not impair MP1o pruning (Figure S5C-S5E). Similarly, RNAi
295 knockdown of Uba1 or Cullin1 (core components of the UPS), which effectively blocks
296 daIV dendrite pruning[21], had no detectable effect on MP1o pruning (Figure S5F-S5G).
297 Although we cannot exclude the possibility that the lack of pruning phenotype may
298 result from insufficient RNAi efficiency, these findings suggest that caspase activity and
299 UPS signaling are not essential for MP1 DAN axon pruning.

300 To identify molecular pathways required for DAN axon pruning, we performed a targeted
301 genetic screen of over 200 fly lines encompassing ~60 candidate genes implicated in
302 neural development and remodeling. This screen revealed a critical role for GSK3β
303 (Shaggy, Sgg in *Drosophila*) in DAN axon pruning. Expression of a dominant-negative
304 form of GSK3β (GSK3β-DN), which mimics GSK3β inhibition, led to a pronounced
305 pruning defect, with persistent axons in the MP1o branch detectable in adult flies
306 (Figure 6A-6B). Given that the GSK3β activity is negatively regulated by AKT[59–61], we
307 asked whether elevated AKT activity similarly impacts pruning. We found that
308 expression of a constitutively active form of AKT (AKT-CA) in MP1 DANs also disrupted
309 MP1o pruning (Figure 6C). In contrast, expression of constitutively active S6K1, a
310 downstream effector of mTORC1[62], did not affect pruning (Figure 6D). These findings
311 suggest a role for AKT-GSK3β signaling, but not mTORC1, in DAN axon pruning.

312 **Differential roles of AKT-GSK3β signaling in neuronal remodeling**

313 We next asked whether AKT-GSK3β signaling is similarly involved in neuronal
314 remodeling in other neuron types, such as MB γ neurons and daIV neurons. We found
315 that expression of AKT-CA or GSK3β-DN in MB γ neurons did not impair γ neuron axon
316 pruning at 18 hr APF (Figure 6E-6F), consistent with previous reports that AKT is not
317 required for γ neuron pruning[16]. Unexpectedly, AKT-CA expression appeared to
318 enhance γ neuron axon pruning, as the distal tips of unpruned γ lobes—clearly visible in
319 controls—was barely detectable in AKT-CA brains (Figure 6E-6F, arrow). Quantification
320 of GFP-labeled pixels confirmed a significant reduction in signal at the distal tip of the
321 vertical lobes in AKT-CA brains compared to wild type (Figure 6H). Additionally, we

322 observed a significant enlargement of the MB junction/MV1 region in AKT-CA flies
323 (Figure 6F, arrowhead, and 6I). These phenotypes were not observed in GSK3β-DN
324 brains (Figure 6G-6I), suggesting that AKT and GSK3β may play distinct roles in γ
325 neuron remodeling.

326 Although RNAi knockdown of AKT has been reported to rescue dendrite pruning defects
327 caused by Cullin1 knockdown in daIV neurons[63], we found that AKT-CA expression did
328 not impair daIV dendrite pruning at 18 hr APF (Figure S6A-S6B), possibly due to context
329 dependent differences in AKT activities. In contrast, expression of GSK3β-DN
330 significantly disrupted daIV dendrite pruning (Figure S6A-S6B), consistent with previous
331 findings[64]. Together, these results reveal the differential roles of AKT-GSK3β signaling in
332 the developmental remodeling of distinct neuron types.

333 **Crosstalk between intrinsic AKT-GSK3β signaling and extrinsic glial activity**
334 **during MP1 DAN axon degeneration**

335 Developmental remodeling involves coordinated interactions between cell-autonomous
336 and non-cell-autonomous mechanisms. To explore potential crosstalk between intrinsic
337 AKT-GSK3β signaling and extrinsic glial responses during MP1o pruning, we analyzed
338 glial dynamics across pruning stages in AKT-CA and GSK3β-DN backgrounds. At 18 hr
339 APF, both AKT-CA and GSK3β-DN brains exhibited a reduction in the number of glial
340 cells in the MP1/MP1o region compared to controls, while glial process infiltration
341 remained largely unchanged (Figure S7A). By 24 hr APF, however, both glial cell
342 number and process infiltration were significantly reduced in AKT-CA and GSK3β-DN
343 brains (Figure 7A-7D). These reductions persisted through 30 hr APF in the GSK3β-DN
344 group and trended toward significance in the AKT-CA group (Figure S7B). Together,
345 these findings suggest that AKT-GSK3β signaling suppresses local glial responses
346 during MP1 DAN axon degeneration, revealing a potential regulatory interaction
347 between intrinsic neuronal signaling and extrinsic glial activity.

348 **AKT-GSK3β signaling regulates microtubule cytoskeleton breakdown during DAN**
349 **axon degeneration**

350 To investigate how AKT-GSK3β signaling may influence DAN axon pruning, we
351 examined its role in regulating microtubule cytoskeleton integrity, which is known to be

352 disrupted prior to glial engulfment in other developmental pruning contexts: In both MB γ
353 neurons and daIV neurons, early microtubule disruption is a hallmark of neural
354 degeneration, with glial engulfment occurring only after microtubule cytoskeleton
355 breakdown[19,54,55,64].

356 We used GFP-tagged αTub84B (GFP-αTub84B) as a marker to visualize the
357 microtubule cytoskeleton in the MP1/MP1o branches during pruning. At 12 hr APF,
358 GFP-αTub84B signal was robustly detected in the MP1o branch, with strong expression
359 in its distal portion (using the unpruned MB junction/MV1 region as reference) (Figure
360 7E). However, by 18 and 24 hr APF, the GFP-αTub84B intensity progressively
361 diminished in the MP1o branch (Figure 7E-7F), consistent with microtubule breakdown
362 during the early phase of axon degeneration[19,54].

363 To determine whether AKT-GSK3β signaling modulates this process, we expressed
364 AKT-CA or GSK3β-DN in MP1 DANs and quantified GFP-αTub84B levels. Both
365 manipulations resulted in significantly elevated GFP-αTub84B signal in the distal MP1o
366 region compared to controls (Figure 7G-7H), suggesting that AKT-GSK3β signaling
367 stabilizes microtubule cytoskeleton during degeneration of MP1 DAN axons. Together,
368 these findings suggest a model that AKT-GSK3β signaling cell-autonomously regulates
369 microtubule cytoskeleton breakdown, thereby modulating glial engagement during DAN
370 axon degeneration.

371 **Discussion**

372 **Atypical developmental remodeling of DANs**

373 This study identifies a previously uncharacterized mode of neuronal remodeling in
374 dopamine neurons (DANs) of *Drosophila melanogaster*. In contrast to the stereotypical
375 pruning-then-regrowth remodeling paradigm observed in most neuron types – including
376 MB neurons, APL neurons, PNs, and daIV neurons[10–14] – MP1 DANs follow an atypical
377 overgrowth-then-pruning trajectory (Figure 1 and S8). This remodeling trajectory is
378 particularly striking given that both MP1 DANs and APL neurons innervate the MB, yet
379 exhibit opposite temporal patterns of remodeling. This atypical mode of remodeling of
380 DAN axons represents a notable deviation from established paradigms and

underscores the heterogeneity and complexity of neuronal remodeling programs in the developing brain.

The MP1o branch emerges within a narrow developmental window and targets the MB MV1, a region known to be spared during MB γ neuron pruning[12,19]. The MP1o branch exhibits presynaptic markers and potential synaptic contacts with MB, suggesting that it may be functionally integrated, albeit transiently. These observations raise intriguing possibilities: MP1 DAN axons in the MP1o branch may transiently modulate MB circuit activity, provide scaffolding for subsequent MB connectivity, or serve as a checkpoint to ensure MB pruning or regrowth fidelity.

**Pruning independent of canonical ecdysone signaling**

Our results indicate that MP1 DANs prune independently of the canonical ecdysone–EcR signaling pathway (Figure 5). This is in stark contrast to most remodeling neurons in *Drosophila*, including MB neurons, PNs, APL neurons, da neurons, and thoracic ventral (Tv) neurons, which show EcR expression and rely on ecdysone signaling to initiate remodeling[10,12–15]. A recent study reports that pruning of Beat-$Va_M$ neurons in the ventral nerve cord (VNC) of *Drosophila* is also ecdysone-independent, although EcR expression is detected in these neurons[65]. In contrast, our data indicate that neither EcR-B1 nor EcR-A is detectable in MP1 DANs. While we cannot fully exclude the possibility that MP1 DANs may respond to ecdysone at levels below our detection threshold or with distinct sensitivity compared to other neuron types, our results nonetheless argue that pruning of MP1 DANs proceeds through mechanisms distinct from the canonical ecdysone-EcR pathway. Together, these findings point to neuron-type–specific pruning triggers and underscore the diversity of remodeling logic across the nervous system[1,2,8,16].

**Role of AKT-GSK3β signaling in DAN axon pruning**

Our genetic screen revealed a critical role for AKT-GSK3β signaling in DAN remodeling (Figure 6). Inhibition of GSK3β or constitutive activation of AKT impairs pruning of the MP1o branch, supporting a model in which the proper regulation of AKT and GSK3β activity is essential for timely DAN axon elimination.

410 Mechanistically, we find that AKT-GSK3β signaling modulates microtubule cytoskeleton
411 breakdown during pruning. Pruning of the MP1o branch is accompanied by progressive
412 microtubule disassembly, a hallmark of early axonal degeneration. Expression of AKT-
413 CA or GSK3β-DN preserves microtubule integrity and inhibits pruning, indicating that
414 cytoskeletal destabilization is a prerequisite for MP1 DAN axon degeneration. Our
415 findings support a model in which AKT-GSK3β regulates the pruning process by
416 modulating microtubule destabilization—a known prerequisite for local axon
417 degeneration[2,19,54].

418 **Context-dependent roles of AKT-GSK3β in neuronal remodeling**

419 The role of AKT-GSK3β signaling in neuronal remodeling appears to be neuron type-
420 specific. This pathway is involved in MP1 DAN axon pruning but is dispensable in MB γ
421 neurons and only partially required in da neuron remodeling (Figure 6). These findings
422 highlight the context-dependent deployment of shared signaling pathways across
423 distinct neuronal populations. AKT-GSK3β signaling may thus serve specialized
424 functions depending on the developmental timing, neurite architecture, and extrinsic
425 cellular environment of the remodeling neurons[2,8,16,20,55,66].

426 **Involvement of glial cells in DAN axon pruning**

427 In parallel to cell-intrinsic mechanisms, we demonstrate that pruning of MP1 DAN axons
428 involves local degeneration and glial activity (Figure 4). Glial cells accumulate in the
429 MP1/MP1o region during the pruning window and extend processes into the region with
430 degenerating axons. Lysosomal markers are enriched within glial processes and
431 colocalize with DAN axon fragments, suggestive of active phagocytosis of degenerating
432 neurites. Inhibition of glial endocytic function via expression of temperature-sensitive
433 *shi*$^{ts}$ impairs pruning and leads to accumulation of axonal debris, consistent with a
434 requirement for glial engulfment in axon clearance. These observations are similar to
435 those in MB γ neuron and da neuron pruning, where glial or epidermal cells act as
436 phagocytes for debris engulfment and clearance[23–25,54].

437 **Crosstalk between intrinsic and extrinsic remodeling mechanisms**

438 We find that AKT-GSK3β signaling modulates not only axon-intrinsic cytoskeletal
439 remodeling but also glial behavior (Figure 7). Expression of AKT-CA or GSK3β-DN in
440 MP1 DANs suppresses both glial cell accumulation and glial process infiltration into the
441 MP1o region. This suggests that cytoskeletal integrity within axons may act as a
442 permissive cue for glial engagement, either by modulating the presentation of
443 phagocytic cues on the axonal membrane or by influencing neuron-glia signaling
444 dynamics. This is consistent with observations in MB γ neurons and da neurons, where
445 microtubule breakdown precedes glial engulfment and may serve as a prerequisite for
446 efficient clearance[23,54,55]. Future studies will be needed to dissect whether glia actively
447 sense microtubule disassembly or respond to other neuron-derived “find-me” or “eat-
448 me” signals that are modulated by AKT-GSK3β signaling[67–69].

449 **Implications for neurodegenerative disease**

450 The identification of AKT-GSK3β and glia-involved local axon degeneration mechanism
451 in DAN remodeling has important implications for neurodegenerative diseases. In PD,
452 DAN axon degeneration often precedes soma loss, following a “dying-back” pattern[49,70–
453 72]. Activation of AKT or inhibition of GSK3β has been shown to suppress axon
454 degeneration and soma loss of DANs in mouse models of PD[26–29]. In addition, AKT
455 promotes axon regeneration through inhibition of GSK3β or by modulating microtubule
456 dynamics[73–75]. Growing evidence also underscores the critical role of glial cells in the
457 pathogenesis of neurodegenerative disorders, including Alzheimer's disease (AD), PD,
458 and Huntington's disease (HD)[76–78].

459 Together, these findings suggest that developmental pruning mechanisms may be co-
460 opted or dysregulated in pathological contexts. Although not the primary focus of this
461 study, our results reveal that DANs are capable of extending new axonal branches even
462 after circuit formation (i.e., during the MP1o overgrowth phase). Elucidating the
463 molecular and cellular mechanisms underlying this axon overgrowth may inform novel
464 therapeutic strategies aimed at promoting DAN axon regeneration in PD.

465 In conclusion, this study defines a novel mode of neuronal remodeling in *Drosophila*
466 DANs, integrating AKT-GSK3β–regulated microtubule destabilization with glial
467 engulfment to drive local DAN axon degeneration. These findings broaden the

468 mechanistic repertoire of developmental pruning and provides a framework for
469 investigating neuron-glia interactions in both healthy development and disease-related
470 neurodegeneration.

471 **Acknowledgments**

472 We thank Y.C Chang, Y. Guo, K. Li, N. C. Noyes, C.F. Teo, A. Yong, X. Ming, M. Zubia,
473 C. Chen, P. Jin, J. Ko, and F. Xie for critical discussion; members of the Jan lab for
474 support and feedback throughout this study; We thank S. Younger, X. Zhai, T. Cheng,
475 and M. Y. L. Fontaine for assistance with fly work and reagents; We also thank C. Han,
476 Janelia Research Campus, and the Bloomington *Drosophila* Stock Center for providing
477 fly lines. This work was supported by NIH grants to Y.N.J. (R35NS097227 and
478 R35NS137312), L.Y.J. (R35NS122110), and R.L.D. (5R35NS097224). Y.N.J. and L.Y.J.
479 are Howard Hughes Medical Institute investigators.

480 **Author contributions**

481 Y.N.J. and L.Y.J. supervised the project. X.Z. conceived and initiated the project while in
482 the laboratory of R.L.D., and continued designed and performed experiments in the
483 laboratories of Y.N.J. and L.Y.J. X.Z. performed immunostainings, the genetic screen,
484 photoactivation experiments, and data analysis. W.C. assisted with experiments in da
485 neurons. Y.W. contributed to sample preparation. X.Y.Z. assisted with the genetic
486 screen. X.T. contributed to data analysis. X.Z. wrote the manuscript with input from all
487 authors.

488 **Declaration of interests**

489 The authors declare no competing interests.

490 **References**

491 1. Luo, L., and O'Leary, D.D.M. (2005). Axon retraction and degeneration in
492 development and disease. Annu. Rev. Neurosci. *28*, 127–156.
493 https://doi.org/10.1146/annurev.neuro.28.061604.135632.

494 2. Riccomagno, M.M., and Kolodkin, A.L. (2015). Sculpting Neural Circuits by Axon and
495 Dendrite Pruning. Annu. Rev. Cell Dev. Biol. *31*, 779–805.
496 https://doi.org/10.1146/annurev-cellbio-100913-013038.

3. Jan, Y.N., and Jan, L.Y. (2010). Branching out: mechanisms of dendritic arborization. Nat Rev Neurosci *11*, 316–328.

4. Faust, T.E., Gunner, G., and Schafer, D.P. (2021). Mechanisms governing activity-dependent synaptic pruning in the developing mammalian CNS. Nat. Rev. Neurosci. *22*, 657–673. https://doi.org/10.1038/s41583-021-00507-y.

5. Cocchi, E., Drago, A., and Serretti, A. (2016). Hippocampal Pruning as a New Theory of Schizophrenia Etiopathogenesis. Mol. Neurobiol. *53*, 2065–2081. https://doi.org/10.1007/s12035-015-9174-6.

6. Thomas, M.S.C., Davis, R., Karmiloff-Smith, A., Knowland, V.C.P., and Charman, T. (2016). The over-pruning hypothesis of autism. Dev. Sci. *19*, 284–305. https://doi.org/10.1111/desc.12303.

7. Ramocki, M.B., and Zoghbi, H.Y. (2008). Failure of neuronal homeostasis results in common neuropsychiatric phenotypes. Nature *455*, 912–918. https://doi.org/10.1038/nature07457.

8. Yaron, A., and Schuldiner, O. (2016). Common and Divergent Mechanisms in Developmental Neuronal Remodeling and Dying Back Neurodegeneration. Curr. Biol. *26*, R628–R639. https://doi.org/10.1016/j.cub.2016.05.025.

9. Hong, S., Beja-Glasser, V.F., Nfonoyim, B.M., Frouin, A., Li, S., Ramakrishnan, S., Merry, K.M., Shi, Q., Rosenthal, A., Barres, B.A., et al. (2016). Complement and microglia mediate early synapse loss in Alzheimer mouse models. Science *352*, 712–716. https://doi.org/10.1126/science.aad8373.

10. Kuo, C.T., Jan, L.Y., and Jan, Y.N. (2005). Dendrite-specific remodeling of Drosophila sensory neurons requires matrix metalloproteases, ubiquitin-proteasome, and ecdysone signaling. Proc. Natl. Acad. Sci. *102*, 15230–15235. https://doi.org/10.1073/pnas.0507393102.

11. Williams, D.W., and Truman, J.W. (2005). Cellular mechanisms of dendrite pruning in Drosophila: insights from in vivo time-lapse of remodeling dendritic arborizing sensory neurons. Development *132*, 3631–3642. https://doi.org/10.1242/dev.01928.

12. Lee, T., Marticke, S., Sung, C., Robinow, S., and Luo, L. (2000). Cell-Autonomous Requirement of the USP/EcR-B Ecdysone Receptor for Mushroom Body Neuronal Remodeling in *Drosophila*. Neuron *28*, 807–818. https://doi.org/10.1016/S0896-6273(00)00155-0.

13. Marin, E.C., Watts, R.J., Tanaka, N.K., Ito, K., and Luo, L. (2005). Developmentally programmed remodeling of the Drosophilaolfactory circuit. Development *132*, 725–737. https://doi.org/10.1242/dev.01614.

14. Mayseless, O., Berns, D.S., Yu, X.M., Riemensperger, T., Fiala, A., and Schuldiner, O. (2018). Developmental Coordination during Olfactory Circuit Remodeling in *Drosophila*. Neuron *99*, 1204-1215.e5. https://doi.org/10.1016/j.neuron.2018.07.050.

15. Schubiger, M., Wade, A.A., Carney, G.E., Truman, J.W., and Bender, M. (1998). Drosophila EcR-B ecdysone receptor isoforms are required for larval molting and for neuron remodeling during metamorphosis. Development *125*, 2053–2062. https://doi.org/10.1242/dev.125.11.2053.

16. Yu, F., and Schuldiner, O. (2014). Axon and dendrite pruning in *Drosophila*. Curr. Opin. Neurobiol. *27*, 192–198. https://doi.org/10.1016/j.conb.2014.04.005.

17. Williams, D.W., Kondo, S., Krzyzanowska, A., Hiromi, Y., and Truman, J.W. (2006). Local caspase activity directs engulfment of dendrites during pruning. Nat. Neurosci. *9*, 1234–1236. https://doi.org/10.1038/nn1774.

18. Kuo, C.T., Zhu, S., Younger, S., Jan, L.Y., and Jan, Y.N. (2006). Identification of E2/E3 Ubiquitinating Enzymes and Caspase Activity Regulating Drosophila Sensory Neuron Dendrite Pruning. Neuron *51*, 283–290. https://doi.org/10.1016/j.neuron.2006.07.014.

19. Watts, R.J., Hoopfer, E.D., and Luo, L. (2003). Axon pruning during Drosophila metamorphosis: evidence for local degeneration and requirement of the ubiquitin-proteasome system. Neuron *38*, 871–885.

20. Awasaki, T., Huang, Y., O'Connor, M.B., and Lee, T. (2011). Glia instruct developmental neuronal remodeling through TGF-Î 2 signaling. Nat. Neurosci. *14*, 821–823. https://doi.org/10.1038/nn.2833.

21. Furusawa, K., Ishii, K., Tsuji, M., Tokumitsu, N., Hasegawa, E., and Emoto, K. (2023). Presynaptic Ube3a E3 ligase promotes synapse elimination through down-regulation of BMP signaling. Science *381*, 1197–1205. https://doi.org/10.1126/science.ade8978.

22. Zheng, X., Wang, J., Haerry, T.E., Wu, A.Y.H., Martin, J., O'Connor, M.B., Lee, C.H.J., and Lee, T. (2003). TGF-β signaling activates steroid hormone receptor expression during neuronal remodeling in the Drosophila brain. Cell *112*, 303–315. https://doi.org/10.1016/S0092-8674(03)00072-2.

23. Watts, R.J., Schuldiner, O., Perrino, J., Larsen, C., and Luo, L. (2004). Glia engulf degenerating axons during developmental axon pruning. Curr. Biol. *14*, 678–684. https://doi.org/10.1016/j.cub.2004.03.035.

24. Awasaki, T., and Ito, K. (2004). Engulfing action of glial cells is required for programmed axon pruning during Drosophila metamorphosis. Curr. Biol. *14*, 668–677. https://doi.org/10.1016/j.cub.2004.04.001.

25. Han, C., Song, Y., Xiao, H., Wang, D., Franc, N.C., Yeh Jan, L., and Jan, Y.N. (2014). Epidermal Cells Are the Primary Phagocytes in the Fragmentation and Clearance of Degenerating Dendrites in Drosophila. Neuron *81*, 544–560. https://doi.org/10.1016/j.neuron.2013.11.021.

26. Cheng, H.-C., Kim, S.R., Oo, T.F., Kareva, T., Yarygina, O., Rzhetskaya, M., Wang, C., During, M., Talloczy, Z., Tanaka, K., et al. (2011). Akt Suppresses Retrograde Degeneration of Dopaminergic Axons by Inhibition of Macroautophagy. J. Neurosci. *31*, 2125–2135. https://doi.org/10.1523/JNEUROSCI.5519-10.2011.

27. Ries, V., Henchcliffe, C., Kareva, T., Rzhetskaya, M., Bland, R., During, M.J., Kholodilov, N., and Burke, R.E. (2006). Oncoprotein Akt/PKB induces trophic effects in murine models of Parkinson's disease. Proc. Natl. Acad. Sci. *103*, 18757–18762. https://doi.org/10.1073/pnas.0606401103.

28. Wang, W., Yang, Y., Ying, C., Li, W., Ruan, H., Zhu, X., You, Y., Han, Y., Chen, R., Wang, Y., et al. (2007). Inhibition of glycogen synthase kinase-3β protects dopaminergic neurons from MPTP toxicity. Neuropharmacology *52*, 1678–1684. https://doi.org/10.1016/j.neuropharm.2007.03.017.

29. Morales-García, J.A., Susín, C., Alonso-Gil, S., Pérez, D.I., Palomo, V., Pérez, C., Conde, S., Santos, A., Gil, C., Martínez, A., et al. (2013). Glycogen Synthase Kinase-3 Inhibitors as Potent Therapeutic Agents for the Treatment of Parkinson Disease. ACS Chem. Neurosci. *4*, 350–360. https://doi.org/10.1021/cn300182g.

30. Mao, Z., and Davis, R.L. (2009). Eight different types of dopaminergic neurons innervate the Drosophila mushroom body neuropil: anatomical and physiological heterogeneity. Front. Neural Circuits *3*.

31. Aso, Y., Hattori, D., Yu, Y., Johnston, R.M., Iyer, N.A., Ngo, T.-T., Dionne, H., Abbott, L., Axel, R., Tanimoto, H., et al. (2014). The neuronal architecture of the mushroom body provides a logic for associative learning. eLife *3*, e04577. https://doi.org/10.7554/elife.04577.

32. Liu, Q., Liu, S., Kodama, L., Driscoll, M.R., and Wu, M.N. (2012). Two dopaminergic neurons signal to the dorsal fan-shaped body to promote wakefulness in Drosophila. Curr Biol *22*, 2114–2123. https://doi.org/10.1016/j.cub.2012.09.008.

33. Marquis, M., and Wilson, R.I. (2022). Locomotor and olfactory responses in dopamine neurons of the *Drosophila* superior-lateral brain. Curr. Biol. *32*, 5406-5414.e5. https://doi.org/10.1016/j.cub.2022.11.008.

34. Claridge-Chang, A., Roorda, R.D., Vrontou, E., Sjulson, L., Li, H., Hirsh, J., and Miesenbock, G. (2009). Writing memories with light-addressable reinforcement circuitry. Cell *139*, 405–415. https://doi.org/10.1016/j.cell.2009.08.034.

35. Berry, J.A., Cervantes-Sandoval, I., Chakraborty, M., and Davis, R.L. (2015). Sleep Facilitates Memory by Blocking Dopamine Neuron-Mediated Forgetting. Cell *161*, 1656–1667. https://doi.org/10.1016/j.cell.2015.05.027.

36. Whitworth, A.J., Theodore, D.A., Greene, J.C., Beneš, H., Wes, P.D., and Pallanck, L.J. (2005). Increased glutathione S-transferase activity rescues dopaminergic neuron loss in a Drosophila model of Parkinson's disease. Proc. Natl. Acad. Sci. *102*, 8024–8029. https://doi.org/10.1073/pnas.0501078102.

37. Coulom, H., and Birman, S. (2004). Chronic Exposure to Rotenone Models Sporadic Parkinson's Disease in Drosophila melanogaster. J. Neurosci. *24*, 10993–10998. https://doi.org/10.1523/JNEUROSCI.2993-04.2004.

38. Park, J., Lee, S.B., Lee, S., Kim, Y., Song, S., Kim, S., Bae, E., Kim, J., Shong, M., Kim, J.-M., et al. (2006). Mitochondrial dysfunction in Drosophila PINK1 mutants is complemented by parkin. Nature *441*, 1157–1161. https://doi.org/10.1038/nature04788.

39. Phan, A., Thomas, C.I., Chakraborty, M., Berry, J.A., Kamasawa, N., and Davis, R.L. (2019). Stromalin Constrains Memory Acquisition by Developmentally Limiting Synaptic Vesicle Pool Size. Neuron *101*, 103-118.e5. https://doi.org/10.1016/j.neuron.2018.11.003.

40. Hige, T., Aso, Y., Modi, M.N., Rubin, G.M., and Turner, G.C. (2015). Heterosynaptic Plasticity Underlies Aversive Olfactory Learning in Drosophila. Neuron *88*, 985–998. https://doi.org/10.1016/j.neuron.2015.11.003.

41. Ruta, V., Datta, S.R., Vasconcelos, M.L., Freeland, J., Looger, L.L., and Axel, R. (2010). A dimorphic pheromone circuit in Drosophila from sensory input to descending output. Nature *468*, 686–690. https://doi.org/10.1038/nature09554.

42. Zhang, X., Sabandal, J.M., Tsaprailis, G., and Davis, R.L. (2022). Active forgetting requires Sickie function in a dedicated dopamine circuit in Drosophila. Proc. Natl. Acad. Sci. *119*, e2204229119. https://doi.org/10.1073/pnas.2204229119.

43. Aso, Y., Siwanowicz, I., Bräcker, L., Ito, K., Kitamoto, T., and Tanimoto, H. (2010). Specific dopaminergic neurons for the formation of labile aversive memory. Curr. Biol. *20*, 1445–1451.

44. Berry, J.A., Cervantes-Sandoval, I., Nicholas, E.P., and Davis, R.L. (2012). Dopamine Is Required for Learning and Forgetting in Drosophila. Neuron *74*, 530–542. https://doi.org/10.1016/j.neuron.2012.04.007.

45. Aso, Y., Herb, A., Ogueta, M., Siwanowicz, I., Templier, T., Friedrich, A.B., Ito, K., Scholz, H., and Tanimoto, H. (2012). Three Dopamine pathways induce aversive odor memories with different stability. PLoS Genet. *8*, e1002768. https://doi.org/10.1371/journal.pgen.1002768.

641 46. Lee, T., Lee, A., and Luo, L. (1999). Development of the Drosophila mushroom
642 bodies: sequential generation of three distinct types of neurons from a neuroblast.
643 Development *126*, 4065–4076.

644 47. Feinberg, E.H., Vanhoven, M.K., Bendesky, A., Wang, G., Fetter, R.D., Shen, K., and
645 Bargmann, C.I. (2008). GFP Reconstitution Across Synaptic Partners (GRASP)
646 defines cell contacts and synapses in living nervous systems. Neuron *57*, 353–363.
647 https://doi.org/10.1016/j.neuron.2007.11.030.

648 48. Wagh, D.A., Rasse, T.M., Asan, E., Hofbauer, A., Schwenkert, I., Dürrbeck, H.,
649 Buchner, S., Dabauvalle, M.C., Schmidt, M., Qin, G., et al. (2006). Bruchpilot, a
650 protein with homology to ELKS/CAST, is required for structural integrity and function
651 of synaptic active zones in Drosophila. Neuron *49*, 833–844.
652 https://doi.org/10.1016/j.neuron.2006.02.008.

653 49. Gcwensa, N.Z., Russell, D.L., Cowell, R.M., and Volpicelli-Daley, L.A. (2021).
654 Molecular Mechanisms Underlying Synaptic and Axon Degeneration in Parkinson's
655 Disease. Front. Cell. Neurosci. *15*.

656 50. Burke, R.E., and O'Malley, K. (2013). Axon degeneration in Parkinson's disease.
657 Exp. Neurol. *246*, 72–83. https://doi.org/10.1016/j.expneurol.2012.01.011.

658 51. Grosch, J., Winkler, J., and Kohl, Z. (2016). Early Degeneration of Both
659 Dopaminergic and Serotonergic Axons – A Common Mechanism in Parkinson's
660 Disease. Front. Cell. Neurosci. *10*.

661 52. Coleman, M.P., and Perry, V.H. (2002). Axon pathology in neurological disease: a
662 neglected therapeutic target. Trends Neurosci. *25*, 532–537.
663 https://doi.org/10.1016/S0166-2236(02)02255-5.

664 53. Raff, M.C., Whitmore, A.V., and Finn, J.T. (2002). Axonal Self-Destruction and
665 Neurodegeneration. Science *296*, 868–871.
666 https://doi.org/10.1126/science.1068613.

667 54. Awasaki, T., Tatsumi, R., Takahashi, K., Arai, K., Nakanishi, Y., Ueda, R., and Ito, K.
668 (2006). Essential Role of the Apoptotic Cell Engulfment Genes draper and ced-6 in
669 Programmed Axon Pruning during Drosophila Metamorphosis. Neuron *50*, 855–867.
670 https://doi.org/10.1016/j.neuron.2006.04.027.

671 55. Lee, H.-H., Jan, L.Y., and Jan, Y.-N. (2009). Drosophila IKK-related kinase Ik2 and
672 Katanin p60-like 1 regulate dendrite pruning of sensory neuron during
673 metamorphosis. Proc. Natl. Acad. Sci. *106*, 6363–6368.
674 https://doi.org/10.1073/pnas.0902051106.

675 56. MacDonald, J.M., Beach, M.G., Porpiglia, E., Sheehan, A.E., Watts, R.J., and
676 Freeman, M.R. (2006). The *Drosophila* Cell Corpse Engulfment Receptor Draper
677 Mediates Glial Clearance of Severed Axons. Neuron *50*, 869–881.
678 https://doi.org/10.1016/j.neuron.2006.04.028.

679 57. Orth, J.D., and McNiven, M.A. (2003). Dynamin at the actin–membrane interface.
680 Curr. Opin. Cell Biol. *15*, 31–39. https://doi.org/10.1016/S0955-0674(02)00010-8.

681 58. Kitamoto, T. (2001). Conditional modification of behavior in Drosophila by targeted
682 expression of a temperature-sensitive shibire allele in defined neurons. J Neurobiol
683 *47*, 81–92.

684 59. Manning, B.D., and Cantley, L.C. (2007). AKT/PKB Signaling: Navigating
685 Downstream. Cell *129*, 1261–1274. https://doi.org/10.1016/j.cell.2007.06.009.

686 60. Cross, D.A.E., Alessi, D.R., Cohen, P., Andjelkovich, M., and Hemmings, B.A.
687 (1995). Inhibition of glycogen synthase kinase-3 by insulin mediated by protein
688 kinase B. Nature *378*, 785–789. https://doi.org/10.1038/378785a0.

689 61. Hermida, M.A., Dinesh Kumar, J., and Leslie, N.R. (2017). GSK3 and its interactions
690 with the PI3K/AKT/mTOR signalling network. Adv. Biol. Regul. *65*, 5–15.
691 https://doi.org/10.1016/j.jbior.2017.06.003.

692 62. Saxton, R.A., and Sabatini, D.M. (2017). mTOR Signaling in Growth, Metabolism,
693 and Disease. Cell *168*, 960–976. https://doi.org/10.1016/j.cell.2017.02.004.

694 63. Wong, J.J.L., Li, S., Lim, E.K.H., Wang, Y., Wang, C., Zhang, H., Kirilly, D., Wu, C.,
695 Liou, Y.-C., Wang, H., et al. (2013). A Cullin1-Based SCF E3 Ubiquitin Ligase
696 Targets the InR/PI3K/TOR Pathway to Regulate Neuronal Pruning. PLOS Biol. *11*,
697 e1001657. https://doi.org/10.1371/journal.pbio.1001657.

698 64. Dzaki, N., Bu, S., Lau, S.S.Y., Yong, W.L., and Yu, F. (2022). Drosophila GSK3β
699 promotes microtubule disassembly and dendrite pruning in sensory neurons.
700 Development *149*, dev200844. https://doi.org/10.1242/dev.200844.

701 65. Lehmann, K.S., Hupp, M.T., Abalde-Atristain, L., Jefferson, A., Cheng, Y.-C.,
702 Sheehan, A.E., Kang, Y., and Freeman, M.R. (2024). Astrocyte-dependent local
703 neurite pruning in Beat-Va neurons. J. Cell Biol. *224*, e202312043.
704 https://doi.org/10.1083/jcb.202312043.

705 66. Awasaki, T., and Lee, T. (2011). Orphan nuclear receptors control neuronal
706 remodeling during fly metamorphosis. Nat. Neurosci. *14*, 6–7.
707 https://doi.org/10.1038/nn0111-6.

708 67. Segawa, K., and Nagata, S. (2015). An Apoptotic 'Eat Me' Signal:
709 Phosphatidylserine Exposure. Trends Cell Biol. *25*, 639–650.
710 https://doi.org/10.1016/j.tcb.2015.08.003.

711 68. Ravichandran, K.S. (2010). Find-me and eat-me signals in apoptotic cell clearance:
712 progress and conundrums. J. Exp. Med. *207*, 1807–1817.
713 https://doi.org/10.1084/jem.20101157.

714 69. Ravichandran, K.S. (2011). Beginnings of a Good Apoptotic Meal: The Find-Me and
715 Eat-Me Signaling Pathways. Immunity *35*, 445–455.
716 https://doi.org/10.1016/j.immuni.2011.09.004.

717 70. Song, P., Peng, W., Sauve, V., Fakih, R., Xie, Z., Ysselstein, D., Krainc, T., Wong,
718 Y.C., Mencacci, N.E., Savas, J.N., et al. (2023). Parkinson's disease-linked parkin
719 mutation disrupts recycling of synaptic vesicles in human dopaminergic neurons.
720 Neuron *111*, 3775-3788.e7. https://doi.org/10.1016/j.neuron.2023.08.018.

721 71. Tagliaferro, P., and Burke, R.E. (2016). Retrograde Axonal Degeneration in
722 Parkinson Disease. J. Park. Dis. *6*, 1–15. https://doi.org/10.3233/JPD-150769.

723 72. Volpicelli-Daley, L.A., Luk, K.C., Patel, T.P., Tanik, S.A., Riddle, D.M., Stieber, A.,
724 Meaney, D.F., Trojanowski, J.Q., and Lee, V.M.-Y. (2011). Exogenous α-Synuclein
725 Fibrils Induce Lewy Body Pathology Leading to Synaptic Dysfunction and Neuron
726 Death. Neuron *72*, 57–71. https://doi.org/10.1016/j.neuron.2011.08.033.

727 73. Song, Y., Ori-McKenney, K.M., Zheng, Y., Han, C., Jan, L.Y., and Jan, Y.N. (2012).
728 Regeneration of Drosophila sensory neuron axons and dendrites is regulated by the
729 Akt pathway involving Pten and microRNA bantam. Genes Dev. *26*, 1612–1625.
730 https://doi.org/10.1101/gad.193243.112.

731 74. Guo, X., Snider, W.D., and Chen, B. (2016). GSK3β regulates AKT-induced central
732 nervous system axon regeneration via an eIF2Bε-dependent, mTORC1-independent
733 pathway. eLife *5*, e11903. https://doi.org/10.7554/eLife.11903.

734 75. Kim, S.R., Chen, X., Oo, T.F., Kareva, T., Yarygina, O., Wang, C., During, M.,
735 Kholodilov, N., and Burke, R.E. (2011). Dopaminergic pathway reconstruction by
736 Akt/Rheb-induced axon regeneration. Ann. Neurol. *70*, 110–120.
737 https://doi.org/10.1002/ana.22383.

738 76. Wilson, D.M., Cookson, M.R., Van Den Bosch, L., Zetterberg, H., Holtzman, D.M.,
739 and Dewachter, I. (2023). Hallmarks of neurodegenerative diseases. Cell *186*, 693–
740 714. https://doi.org/10.1016/j.cell.2022.12.032.

741 77. Hanslik, K.L., Marino, K.M., and Ulland, T.K. (2021). Modulation of Glial Function in
742 Health, Aging, and Neurodegenerative Disease. Front. Cell. Neurosci. *15*.
743 https://doi.org/10.3389/fncel.2021.718324.

744 78. Glass, C.K., Saijo, K., Winner, B., Marchetto, M.C., and Gage, F.H. (2010).
745 Mechanisms Underlying Inflammation in Neurodegeneration. Cell *140*, 918–934.
746 https://doi.org/10.1016/j.cell.2010.02.016.

747 79. Han, C., Jan, L.Y., and Jan, Y.-N. (2011). Enhancer-driven membrane markers for
748 analysis of nonautonomous mechanisms reveal neuron–glia interactions in
749 Drosophila. Proc. Natl. Acad. Sci. *108*, 9673–9678.
750 https://doi.org/10.1073/pnas.1106386108.

751 80. Lee, T., and Luo, L. (1999). Mosaic analysis with a repressible cell marker for
752 studies of gene function in neuronal morphogenesis. Neuron *22*, 451–461.

753 81. Pech, U., Pooryasin, A., Birman, S., and Fiala, A. (2013). Localization of the
754 Contacts Between Kenyon Cells and Aminergic Neurons in the Drosophila
755 melanogaster Brain Using SplitGFP Reconstitution. J. Comp. Neurol. *521*, 3992–
756 4026. https://doi.org/10.1002/CNE.23388.

757 82. Yadav, S., Younger, S.H., Zhang, L., Thompson-Peer, K.L., Li, T., Jan, L.Y., and Jan,
758 Y.N. (2019). Glial ensheathment of the somatodendritic compartment regulates
759 sensory neuron structure and activity. Proc. Natl. Acad. Sci. U. S. A. *116*, 5126–
760 5134.

761 83. Jenett, A., Rubin, G.M., Ngo, T.T.B., Shepherd, D., Murphy, C., Dionne, H., Pfeiffer,
762 B.D., Cavallaro, A., Hall, D., Jeter, J., et al. (2012). A GAL4-Driver Line Resource for
763 Drosophila Neurobiology. Cell Rep. *2*, 991–1001.
764 https://doi.org/10.1016/j.celrep.2012.09.011.

765

766

767 **RESOURCE AVAILABILITY**

768 Further information and requests for resources and reagents should be directed to the
769 lead contact Yuh Nung Jan (yuhnung.jan@ucsf.edu).

770 **Materials availability**

771 All unique reagents generated in this study are available from the lead contact.

772 **Data and code availability**

773 This study does not generate datasets or code.

774 **EXPERIMENTAL MODEL AND STUDY PARTICIPANT DETAILS**

775 ***Drosophila* husbandry and strains**

776 Flies were maintained on standard *Drosophila* food at 25°C, 70% relative humidity,
777 under a 12/12 hr light/dark cycle unless otherwise specified. Pupae were collected at 2
778 hr intervals and aged to defined developmental stages for subsequent experiments. The
779 following fly strains were used: w1118, TH-D'-Gal4 driver[32], MB320C-Split-Gal4 driver[40],
780 UAS-CD4-tdTomato[79], UAS-CD4-tdGFP[79], UAS-mCD8-GFP[80], UAS-myr-GFP (BDSC
781 #32197), UAS-myrGFP.QUAS-mtdTomato-3xHA (BDSC #77479), UAS-C3PA-GFP[41],
782 MB-spGFP11 construct[81], UAS-spGFP1-10 construct[47], UAS-Brp-GFP (gift from
783 Stephan Sigrist), RedRepo[82], Repo-QF2 (BDSC #66477), QUAS-shi$^{ts1}$ (BDSC #30013),
784 UAS-EcR-B1$^{DN}$ (BDSC# 6872), UAS-EcR-A$^{DN}$ (BDSC #9452), UAS-AKT$^{CA}$ (BDSC
785 #80935), UAS-GSK3β$^{DN}$ (BDSC #5360), UAS-S6K$^{CA}$ (BDSC #6913), 201y-Gal4 (BDSC
786 #64296), PPK-Gal4 driver[79], UAS-GFP-αTub84B (BDSC #7373), UAS-Dronc$^{DN}$ (BDSC
787 #58992), UAS-p35 (BDSC #5073), UAS-DIAP1 (BDSC #6657), TRiP RNAi control lines
788 (BDSC# 36303 or 36304), UAS-Uba1-RNAi (BDSC #76066), UAS-Cullin1-RNAi (BDSC
789 #29520). Genotypes of flies in each experiment are described in Table S1.

790 **Immunostaining**

791 Drosophila brains were dissected and processed as previously described[42,83]. Briefly,
792 brains were dissected in cold S2 medium (Life Technologies, Cat# 21720-024) and fixed
793 overnight at 4°C in 1% paraformaldehyde in S2 medium. Following fixation, brains were

794 washed with PAT3 buffer [phosphate buffered saline (PBS) with 0.5% BSA and 0.5%
795 TritonX-100], blocked in 3% normal goat serum (NGS) in PAT3, and incubated with
796 primary antibodies diluted in blocking buffer (3% NGS in PAT3) for 3 hours at 23°C,
797 followed by overnight incubation at 4°C. After washing with PAT3, brains were incubated
798 with secondary antibodies in blocking buffer for 3 hours at 23°C and then at 4°C for an
799 additional 5 days. Brains were then washed with PAT3 and subsequently with 1XPBS
800 before mounting with mounting medium (Vector Laboratories, Cat# H-1000-10). Primary
801 antibodies used were: rabbit anti-GFP (1:1000, Invitrogen, Cat# A11122), chicken anti-
802 GFP (1:1000, Abcam, Cat# ab13970), rabbit anti-Dsred (1:1000, Takara Bio, Cat#
803 632496), rabbit anti-TH (1:500, Millipore, Cat# AB152), mouse monoclonal anti-FasII
804 (1:100, DSHB, 1D4, RRID:AB_528235), mouse monoclonal anti-nc82 (1:50, DSHB,
805 RRID:AB_2314866), mouse monoclonal anti-repo (1:100, DSHB, 8D12,
806 RRID:AB_528448), mouse monoclonal anti-EcR-B1 (1:50, DSHB, AD4.4,
807 RRID:AB_2154902), mouse monoclonal anti-EcR-A (1:50, DSHB, 15G1a,
808 RRID:AB_528214). Secondary antibodies used were: Alexa 488 goat anti-rabbit (1:800,
809 Invitrogen, Cat# A11008), Alexa 488 goat anti-chicken (1:800, Invitrogen, Cat# A11039),
810 Alexa 594 donkey anti-mouse (1:500, Jackson Labs, Cat# 715-585-150), Alexa 633
811 goat anti-rabbit (1:800, Invitrogen, Cat# A21070), Alexa 633 goat anti-mouse (1:800,
812 Invitrogen, Cat# A21052). Images were collected on a Leica SP8 confocal microscope
813 using either a 10X dry or 40X oil objective, at 1024 X 1024 or 2048 X 2048-pixel
814 resolution, with excitation lasers at 488, 594, and/or 633 nm. Image analysis was
815 performed using Fiji/ImageJ.
816
817 **LysoTracker staining**

818 Drosophila brains were dissected in S2 medium at room temperature and transferred to
819 100 nM LysoTracker Deep Red (Invitrogen, Cat# L12492) diluted in S2 medium.
820 Samples were incubated for 15 min at room temperature, then washed three times with
821 PBS before imaging.
822
823 **Photoactivation of C3PA-GFP**

824 To label MP1 or MP1o branch with C3PA-GFP, brains were dissected in 1XPBS and
825 transferred to fresh 1XPBS on a microscope slide with a donut-shaped spacer. A
826 coverslip was then applied to the spacer to minimize PBS evaporation and prevent brain
827 movement during subsequent photoactivation and imaging. Prior to photoactivation,
828 MP1 and/or MP1o branches were imaged using a 10X dry objective at 1024 X 1024-
829 pixel resolution with 488 nm (for C3PA-GFP) and/or 561 nm (for tdTomato) laser
830 excitation (designated as the "Pre" image). Photoactivation was performed on a Leica
831 SP8 microscope using a 405 nm laser. TdTomato signal was used to identify the MP1 or
832 MP1o region, and a circular ROI of the same size across experiments was drawn within
833 the boundaries of the MP1 or MP1o region for photoactivation. C3PA-GFP was
834 photoactivated by scanning the ROI with 4 iterations, each lasting 1.471seconds. In
835 experiments requiring visualization of GFP diffusion from axons to soma or soma to
836 axons, the photoactivation protocol was repeated every 10 or 20 minutes to enhance
837 GFP signal for diffusion. After photoactivation, the MP1, MP1o, and/or soma were
838 imaged at defined time points using the same imaging settings as that for the "Pre"
839 image.

840 ***Shi$^{ts}$* experiments**

841 To inhibit dynamin function using *shi$^{ts}$*, pupae cultured at 23°C were shifted to 29°C from
842 approximately 7 hr APF to 24 hr APF. Pupae were dissected at 24 hr APF immediately
843 after removal from 29°C, then fixed and stained as described above.

844 **3D rendering**

845 Three-dimensional reconstruction of the MP1/MP1o branch and MB axons (Video S1)
846 was performed using Imaris software (version 10.1, Bitplane).

847 **Quantification and statistical analysis**

848 Confocal images were analyzed using Fiji/ImageJ, and statistical analyses were
849 performed in GraphPad Prism 9. The sample size for each group, *p*-values and the
850 statistical tests employed for each experiment are indicated in the figures or figure
851 legends.

852 To quantify the relative area occupied by MP1/MP1o (Figure 1), Z-projections were
853 generated from confocal image stacks, and brightness and contrast were adjusted
854 uniformly across all developmental stages. Regions within the MP1/MP1o area with
855 signal above a defined threshold were outlined and measured in Fiji/ImageJ. The
856 resulting area was then normalized to brain size, estimated as the distance between the
857 left and right MP1 branches, to calculate the relative area occupied by MP1/MP1o.

858 To quantify C3PA-GFP fluorescence intensity before and after photoactivation (Figure 2,
859 S2), a circular ROI of the same size was drawn around the outer boundaries of the
860 MP1, MP1o, or soma region for each corresponding area, and the mean intensity was
861 used for quantification.

862 To quantify the number of glial cells in the MP1/MP1o region, Z-projections were
863 generated from confocal stacks. A circular ROI of the same size across all
864 developmental stages was drawn around the outer boundaries of the MP1 and MP1o
865 region, and the number of glial cells within the ROI was counted using Fiji/ImageJ.

866 To quantify glial process intensity, a Z-projection consisting of 15 optical slices (15 μm
867 total) spanning the anterior-posterior extent of the MP1o branch was generated from
868 confocal stacks. A circular ROI of the same size was drawn within the MP1o
869 boundaries, and the mean intensity within the ROI was measured using Fiji/ImageJ.

870 To quantify GFP puncta in the *shi*$^{ts}$ experiments (Figure 4F and 4H), a Z-projection
871 spanning the anterior-posterior extent of the MP1o branch was generated from confocal
872 stacks and converted to greyscale in Fiji/ImageJ. Two duplicate images were created for
873 each projection and subjected to Gaussian blur filter with Sigma values of 1 and 2,
874 respectively. The image with Sigma = 2 was then subtracted from the image with Sigma
875 = 1 using the Image Calculator tool. Thresholding was then applied using the
876 MaxEntropy algorithm, which we found to be the most reliable for distinguishing true
877 GFP puncta from background and false-positive signals. Only GFP puncta located in the
878 distal region of the MP1o branch were quantified, as puncta in the proximal region were
879 predominantly false positives.

To quantify the size of unpruned γ lobe vertical tips and MB peduncles (Figure 6), Z-projections were generated from confocal stacks, and brightness and contrast were adjusted uniformly across all groups. Regions corresponding to the γ lobe vertical tip or MB peduncle with signal above a defined threshold were outlined and measured using Fiji/ImageJ.

To quantify dendrite length (Figure S6), the Simple Neurite Tracer (SNT) plugin in Fiji/ImageJ was used. The total length of all traced dendrites per brain was quantified.

To quantify GFP–αTub84B intensity (Figure 7), a Z-projection consisting of 15 optical slices (15 μm total) spanning the anterior-posterior extent of the MP1o branch was generated from confocal stacks. A rectangular ROI of the same size across all experimental groups was placed around the distal part of the MP1o branch using the unpruned MB peduncle as reference. The mean intensity within the ROI was measured using Fiji/ImageJ after background subtraction using an identical ROI placed in a background region of the image.

895 **Table S1**

| Figure | Panel | Genotype |
|---|---|---|
| Figure 1 | B-I | TH-D'-GAL4/+; UAS-CD4-tdTomato/+ |
| Figure 2 | A-F | TH-D’-GAL4/UAS-C3PA-GFP; UAS-CD4-tdTomato/+ |
| Figure 3 | A-C | TH-D'-GAL4/+; UAS-CD4-tdTomato/+ |
| | D | TH-D'-GAL4/+; MB-spGFP11, UAS-spGFP1-10/+ |
| | E | TH-D’-GAL4/+; UAS-Brp-GFP/UAS-CD4-tdTomato |
| Figure 4 | A, B | TH-D'-GAL4/+; UAS-CD4-tdGFP/+ |
| | C, D | UAS-mCD8-GFP/+; TH-D'-GAL4/Red-Repo |
| | E | TH-D'-GAL4/Red-Repo; UAS-CD4-tdGFP/+ |
| | F-H | UAS-myr-GFP, QUAS-mtdTomato-3xHA/+; TH-D'-GAL4/+ or QUAS-shi$^{ts}$; Repo-QF2/+ |
| Figure 5 | A | UAS-mCD8-GFP/+; UAS-EcR-B1-DN/+; MB320C-GAL4/+ |
| | B | UAS-mCD8-GFP/+; UAS-EcR-A-DN/+; MB320C-GAL4/+ |
| | C, D | UAS-mCD8-GFP/+; TH-D'-GAL4/+ |
| Figure 6 | A | UAS-mCD8-GFP/+;; MB320C-GAL4/+ |
| | B | UAS-mCD8-GFP/+;; MB320C-GAL4/UAS-AKT-CA |
| | C | UAS-mCD8-GFP/+;; MB320C-GAL4/UAS-GSK3β-DN |
| | D | UAS-mCD8-GFP/+;; MB320C-GAL4/UAS-S6K-CA |
| | E-I | 201Y-GAL4, UAS-mCD8-GFP/+, UAS-AKT-CA, or UAS-GSK3β-DN |
| Figure 7 | A-D | UAS-mCD8-GFP/+; TH-D'-GAL4/Red-Repo; +/+, UAS-AKT-CA, or UAS-GSK3β-DN |
| | E, F | TH-D'-GAL4/+; UAS-GFP-αTub84B/+ |
| | G, H | TH-D'-GAL4/+; UAS-GFP-αTub84B/+, UAS-AKT-CA, or UAS-GSK3β-DN |
| Figure S1 | B | TH-D'-GAL4/+; UAS-CD4-tdTomato/+ |
| | C | MB320C-GAL4/UAS-CD4-tdTomato |
| Figure S2 | A, B | UAS-mCD8-GFP/+; TH-D'-GAL4/+ |

| | | |
|---|---|---|
| | C, D | TH-D’-GAL4/UAS-C3PA-GFP; UAS-CD4-tdTomato/+ |
| | E, F | UAS-C3PA-GFP/+; MB320C-GAL4/UAS-CD4-tdTomato |
| Figure S3 | A, B | TH-D'-GAL4/+; UAS-CD4-tdTomato/+ |
| | C | TH-D'-GAL4/+; MB-spGFP11, UAS-spGFP1-10/+ |
| | D | TH-D’-GAL4/+; UAS-Brp-GFP/UAS-CD4-tdTomato |
| Figure S4 | A, B | TH-D'-GAL4/Red-Repo; UAS-CD4-tdGFP/+ |
| Figure S5 | A | 201Y-GAL4, UAS-mCD8-GFP/UAS-EcR-B1-DN |
| | B | UAS-mCD8-GFP/+; TH-D'-GAL4/+ |
| | C | UAS-mCD8-GFP/+; UAS-Dronc-DN/+; MB320C-GAL4/+ |
| | D | UAS-mCD8-GFP/+;; MB320C-GAL4/UAS-p35 |
| | E | UAS-mCD8-GFP/+;; MB320C-GAL4/UAS-DIAP1 |
| | F | UAS-mCD8-GFP/+;; MB320C-GAL4/UAS-Uba1-RNAi |
| | G | UAS-mCD8-GFP/+;; MB320C-GAL4/UAS-Cullin1-RNAi |
| Figure S6 | A, B | PPK-GAL4, UAS-CD4-tdTomato/+, UAS-AKT-CA, or UAS-GSK3β-DN |
| Figure S7 | A, B | UAS-mCD8-GFP/+; TH-D'-GAL4/Red-Repo; +/+, UAS-AKT-CA, or UAS-GSK3β-DN |

896

897

898

## Main Figures

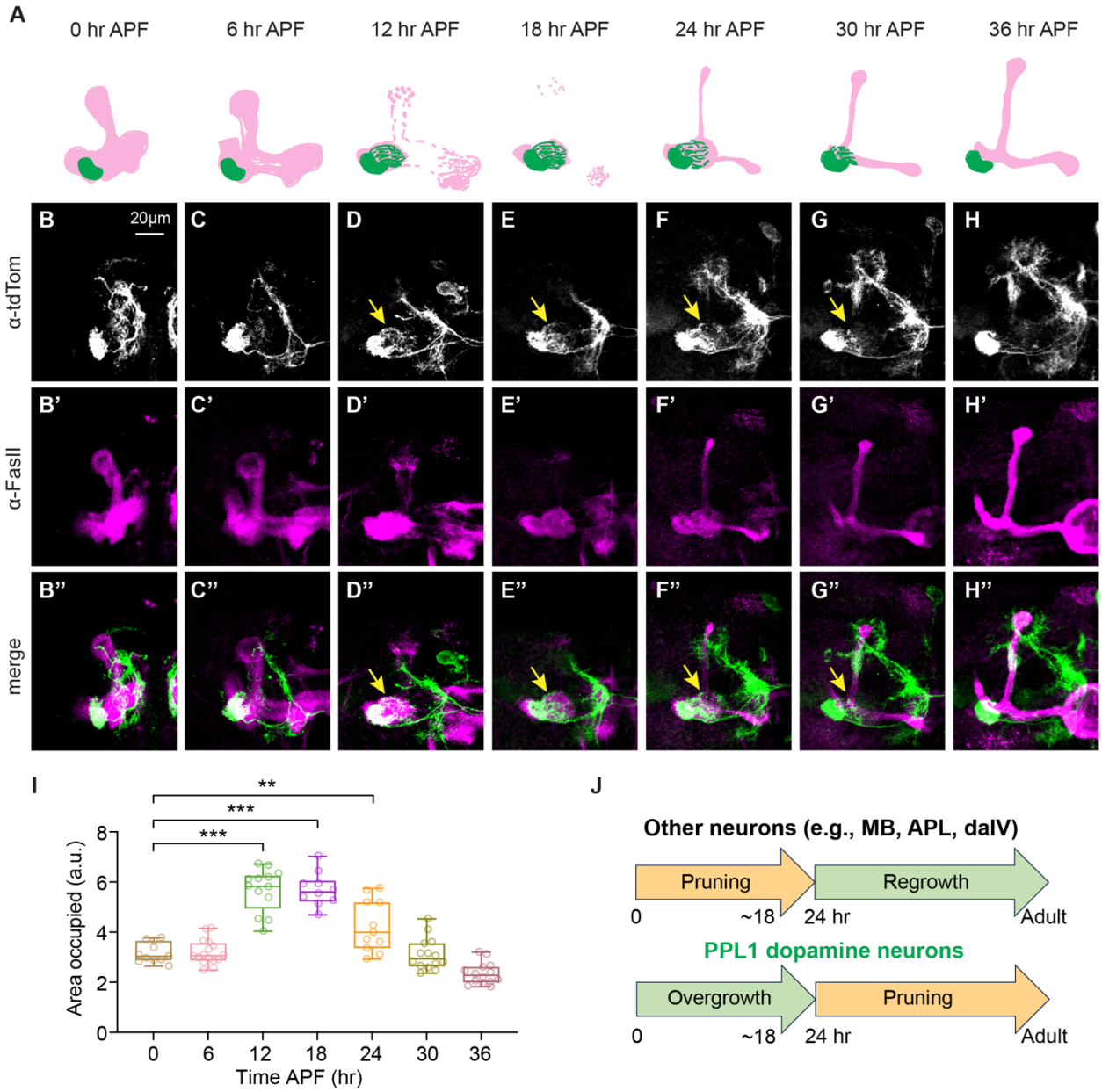


**Figure 1. Atypical developmental remodeling of dopamine neurons**

(A) Schematic of PPL1 DAN axon remodeling during metamorphosis. Green: MP1/MP1o branch; Magenta: Mushroom body (MB) lobes labeled with anti-FasII.

(B-H) Confocal Z projections of brains at 0 hr (B), 6 hr (C), 12 hr (D), 18 hr (E), 24 hr (F), 30 hr (G), and 36 hr (H) APF expressing CD4-tdTomato driven by TH-D'-Gal4; MB

906 lobes are labeled with anti-FasII (B'-H'). Yellow arrows indicate the transient MP1o
907 branch overextending from the MP1 branch into the MB MV1 region. See also Figure
908 S1A-S1B.

909 (I) Quantification of the relative area occupied by MP1/MP1o branch across timepoints.
910 $^{**}p < 0.01$, $^{***}p < 0.001$; $n$ = 10-16. One-way ANOVA with Dunnett's multiple
911 comparisons test.

912 (J) Summary schematic of atypical overgrowth-then-pruning developmental remodeling
913 of DANs.

914

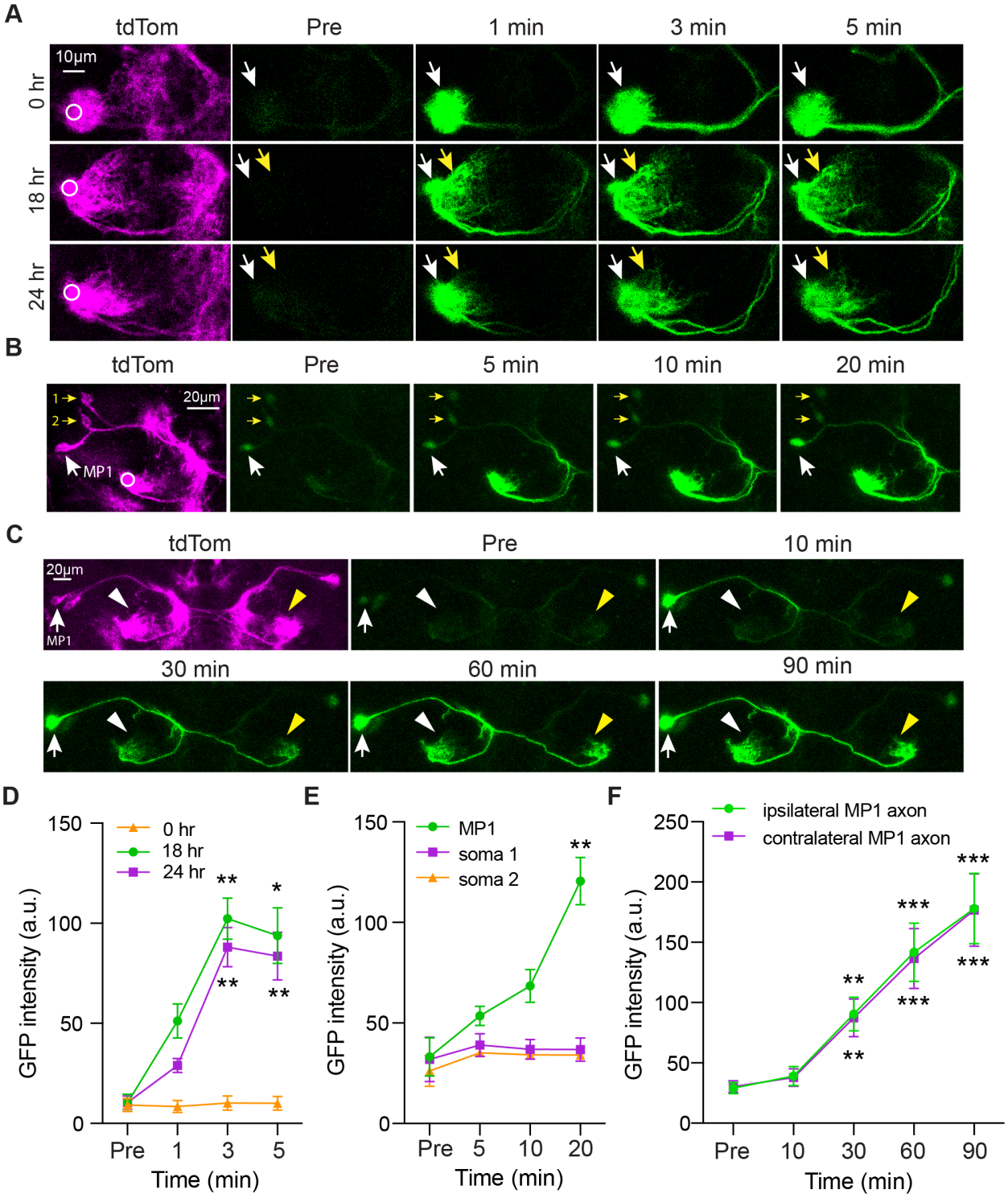


915

916 **Figure 2. A single pair of DANs undergoes atypical developmental remodeling**

917 (A) Photoactivation of C3PA-GFP in the MP1 branch and monitor GFP diffusion to the
918 MP1o region at 0, 18, and 24 hr APF. White circle: ROI for photoactivation; white arrow:
919 MP1 branch region; yellow arrow: MP1o region.

920 (B) Photoactivation in the MP1 branch and monitor GFP diffusion to somas at 18 hr
921 APF. White circle: ROI for photoactivation. White arrow: MP1 soma; yellow arrows: non-
922 MP1 somas.

923 (C) Photoactivation in MP1 soma and monitor GFP diffusion to axons at 18 hr APF.
924 White arrow: MP1 soma; arrowheads: ipsilateral (white) and contralateral (yellow) MP1
925 axons.

926 (D) Quantitation of GFP fluorescence intensity in the MP1o region in (A) before (Pre)
927 and after (1-5 min) photoactivation. *$p < 0.05$, **$p < 0.01$ vs. Pre; $n = 3$-4; mean ± SEM;
928 Repeated measures one-way ANOVA with Dunnett's test.

929 (E) Quantitation of GFP fluorescence intensity in MP1 and two non-MP1 somas in (B)
930 before (Pre) and after (5-20 min) photoactivation. **$p < 0.01$ vs. Pre; $n = 3$; mean ±
931 SEM; Repeated measures one-way ANOVA with Dunnett's test.

932 (F) Quantitation of GFP fluorescence intensity in MP1 axons in (C) before (Pre) and
933 after (10-90 min) photoactivation. **$p < 0.01$, ***$p < 0.001$ vs. Pre; $n = 5$; mean ± SEM;
934 Repeated measures one-way ANOVA with Dunnett's test.

935

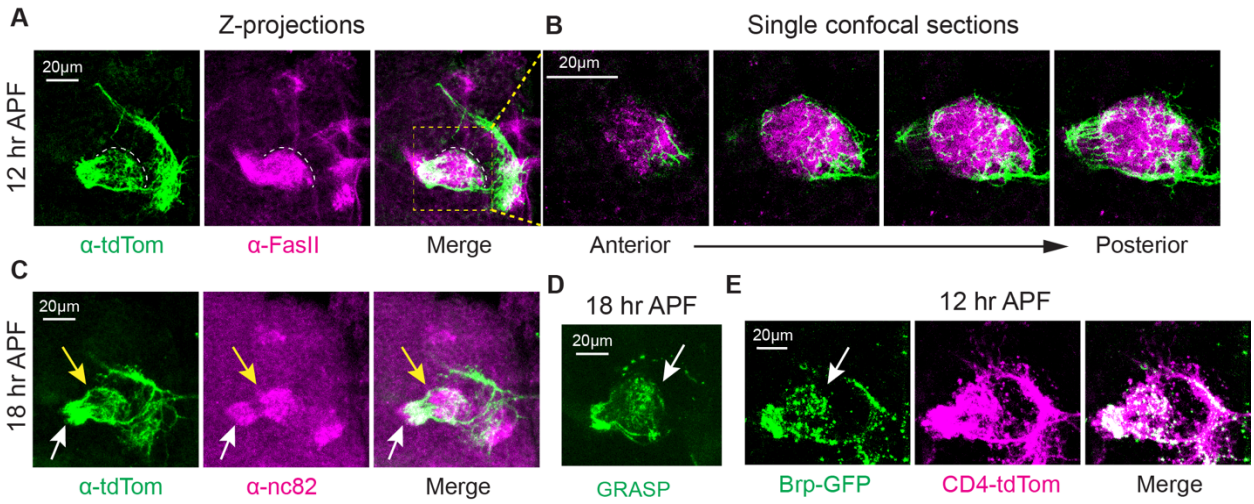


**Figure 3. MP1o targets and is presynaptic to the MB**

(A) Confocal Z projections of brains at 12 hr APF showing MP1o branch (TH-D'>CD4-tdTomato) innervating the MB. MB lobes are labeled with anti-FasII. Dashed lines mark the distal part of MP1o branch and the boundary of degenerating MB junction/MV1 region.

(B) High magnification single confocal sections showing the innervation pattern of MP1o branch in MB MV1 region as in the dashed box in (A).

(C) Confocal Z projections of brains at 18 hr APF expressing CD4-tdTomato driven by TH-D'-Gal4. Brain and MB lobes are visualized with anti-nc82. White arrow: MP1 region; yellow arrow: MP1o and MB MV1 regions.

(D) Confocal Z projections showing GRASP signal between MP1/MP1o and MB at 18 hr APF. White arrow: MP1o region.

(E) Confocal Z projections of brains at 12 hr APF expressing Brp-GFP and CD4-tdTomato driven by TH-D'-Gal4. White arrow: MP1o region.

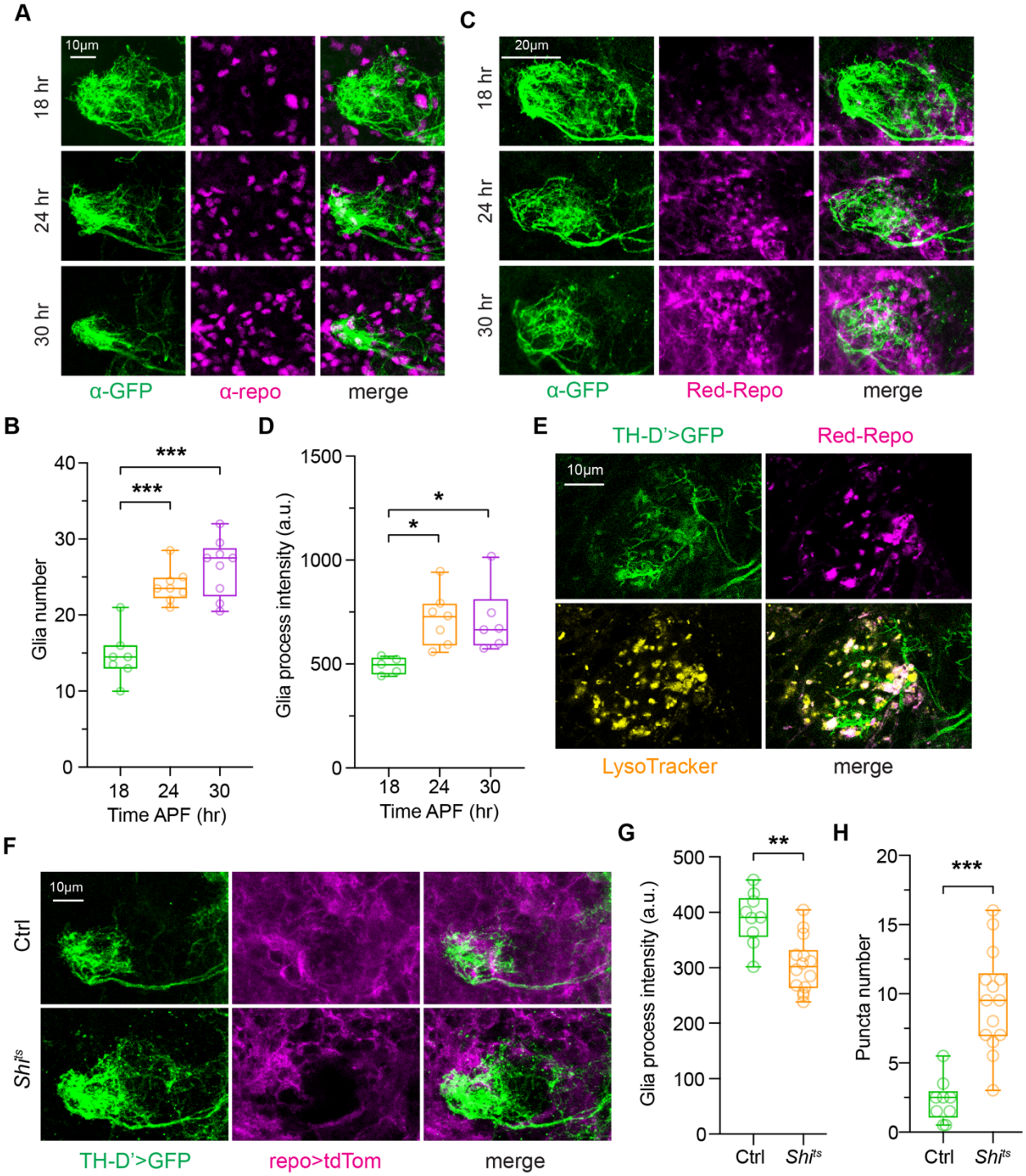


953

954 **Figure 4. Local degeneration and glial involvement in MP1 DAN axon pruning**

955

956 (A) Confocal Z projections of brains at 18 hr (top), 24 hr (middle), and 30 hr (bottom)
957 APF expressing CD4-tdGFP driven by TH-D'-Gal4. Glial nuclei are labeled with anti-
958 Repo.

959 (B) Quantitation of glial cell numbers in the MP1/MP1o region in (A). ***$p < 0.001$; $n = 7$-
960 9; One-way ANOVA with Dunnett's multiple comparisons test.

961 (C) Confocal Z projections of brains at 18 hr (top), 24 hr (middle), and 30 hr (bottom)
962 APF expressing mCD8-GFP driven by TH-D'-Gal4. Glial cells/processes are labeled
963 with Red-Repo.

964 (D) Quantitation of glial process in the MP1o region in (C). *$p < 0.05$; $n = 5$-7; One-way
965 ANOVA with Dunnett's multiple comparisons test.

966 (E) Single confocal section showing MP1/MP1o branch (TH-D'>GFP), glial processes
967 (Red-Repo), LysoTracker, and together (merge) at 24 hr APF. See also Figure S4.

968 (F) Confocal Z projections of brains at 24 hr APF in control (top) and *shi*$^{ts}$ (bottom)
969 groups. MP1 DANs labeled with TH-D'-GAL4>UAS-myr-GFP; glia labeled with Repo-
970 QF2>QUAS-mtdTomato-3XHA, with or without QUAS-*shi*$^{ts}$; Control group lacking
971 QUAS-*shi*$^{ts}$ was subjected to the same temperature shift protocol as *shi*$^{ts}$ group.

972 (G-H) Quantitation of glial process (G) and GFP-positive puncta (H) in MP1o region in
973 (F). **$p < 0.01$, ***$p < 0.001$; $n = 9$-14; Mann Whitney test.

974

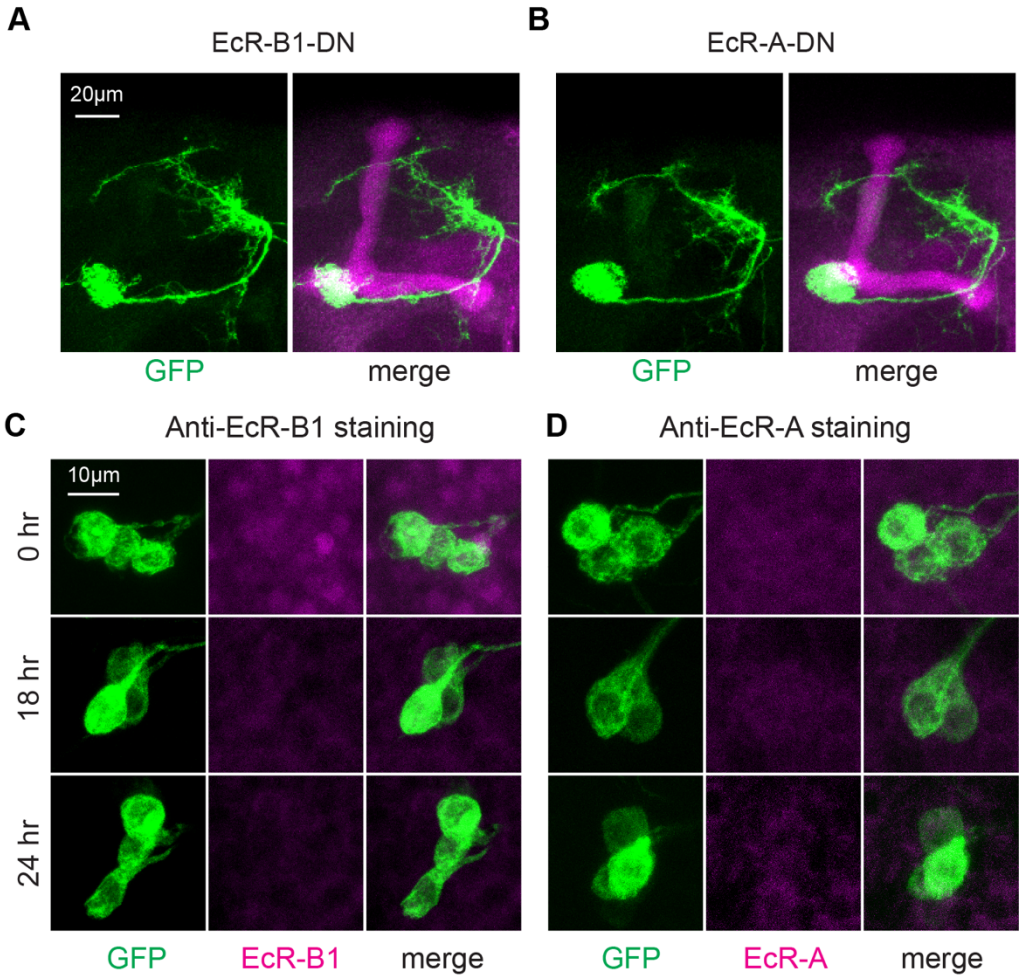


975

976 **Figure 5. Canonical ecdysone signaling is dispensable for DAN axon pruning**

977 (A-B) Confocal Z projections of adult brains expressing mCD8-GFP and EcR-B1-DN (A)
978 or EcR-A-DN (B) driven by MB320C-Gal4. Magenta: MB lobes labeled with anti-FasII.
979 No MP1o branches observed.

980 (C-D) Confocal Z projections of brains at 0 hr (top), 18 hr (middle), and 24 hr (bottom)
981 APF showing somas of MP1 DANs (TH-D'>mCD8-GFP) and immunostaining for EcR-
982 B1 or EcR-A (D). EcR expression is not detected above background in MP1 DANs at
983 any time point. See also Figure S5.

984

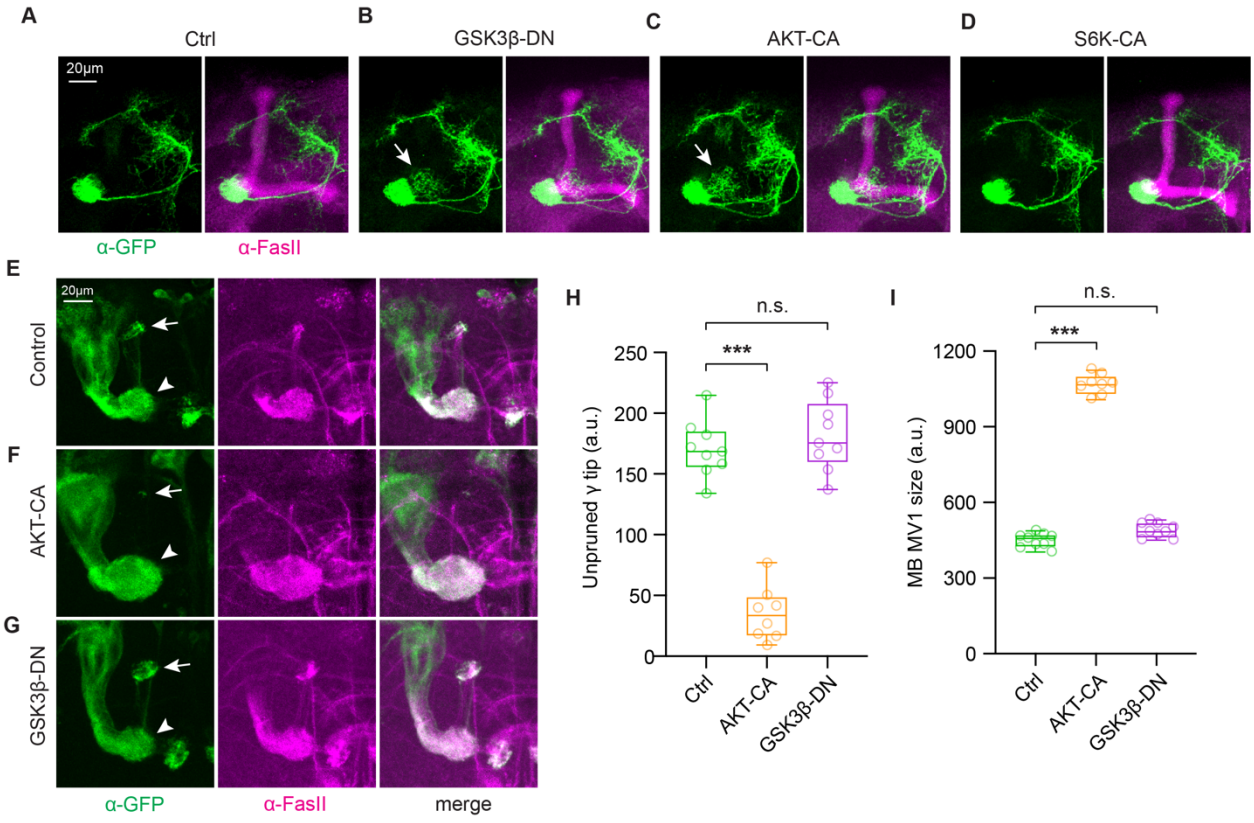


**Figure 6. Roles of AKT-GSK3β signaling in developmental remodeling**

(A-D) Confocal Z projections of adult brains expressing mCD8-GFP driven by MB320C-Gal4. Expression of GSK3β-DN (B) and AKT-CA (C), but not S6K-CA (D) in MP1 DANs impairs pruning of MP1o branch compared to control (A). MB lobes labeled with anti-FasII. White arrow indicates persistent MP1o branch in GSK3β-DN and AKT-CA groups.

(E-G) Differential effects of AKT-CA (F) and GSK3β-DN (G) on MB γ neuron pruning. MB labeled with 201Y-Gal4>mCD8-GFP. White arrow: distal tip of MB γ neuron vertical lobe; white arrowhead: unpruned MB junction/MV1 region.

(H-I) Quantitation of the unpruned distal tip of MB vertical lobe (H) and junction/MV1 area (I) in control (E), AKT-CA (F), and GSK3β-DN (G) groups at 18 hr APF. ***$p < 0.001$; n.s., not significant; $n$ = 8-9; One-way ANOVA with Dunnett's multiple comparisons test.

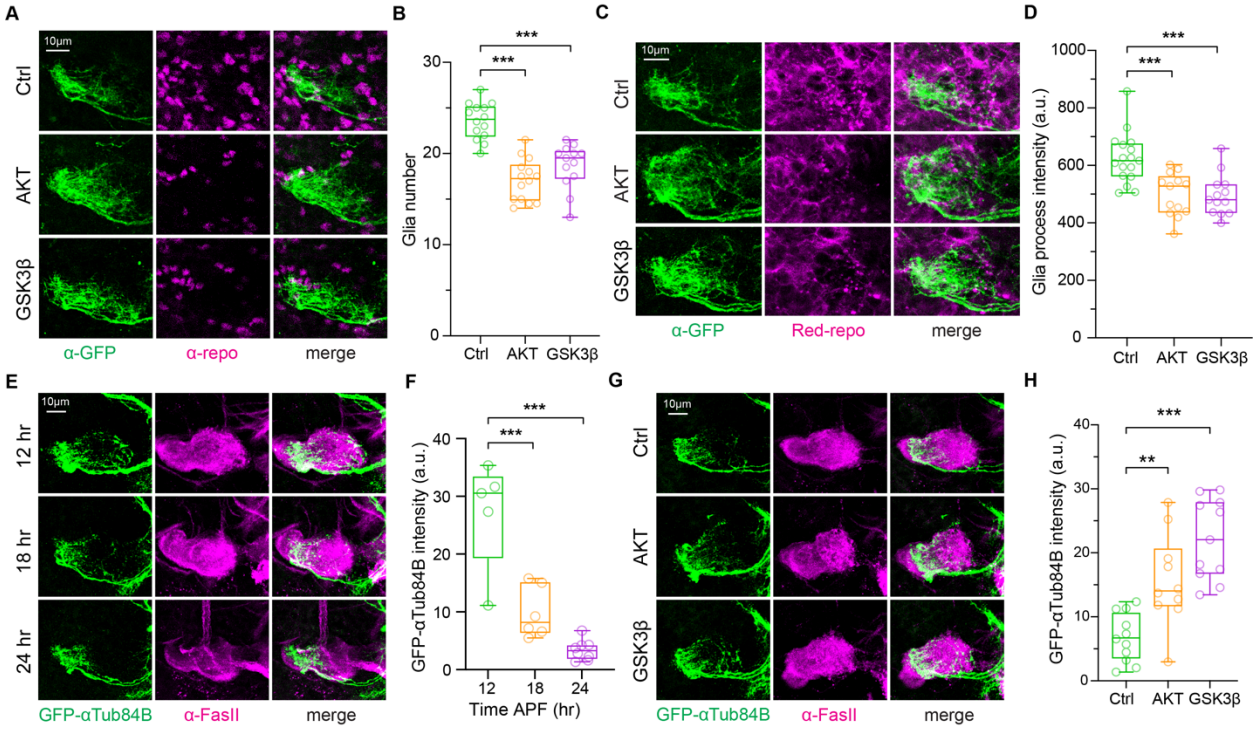


998

999 **Figure 7. AKT-GSK3β signaling modulates microtubule cytoskeleton and glial**
1000 **activities during DAN axon degeneration**

1001 (A) Confocal Z projections of brains at 24 hr APF expressing mCD8-GFP driven by TH-
1002 D'-Gal4 in control (top), AKT-CA (middle), and GSK3β-DN (bottom) groups. Glial nuclei
1003 labeled with anti-Repo.

1004 (B) Quantitation of glial cell number in MP1/MP1o region in (A). ***$p < 0.001$; $n$ = 13-14;
1005 One-way ANOVA with Dunnett's multiple comparisons test.

1006 (C) Confocal Z projections as in (A) but with glial cells/processes labeled with Red-
1007 Repo.

1008 (D) Quantitation of glial process in MP1o region in (C). ***$p < 0.001$; $n$ = 13-17; One-
1009 way ANOVA with Dunnett's multiple comparisons test.

1010 (E) Confocal Z projections of brains at 12 hr (top), 18 hr (middle), and 24 hr (bottom)
1011 APF expressing GFP-αTub84B driven by TH-D'-Gal4. MB lobes labeled with anti-FasII.

1012 (F) Quantitation of GFP-αTub84B signal intensity in MP1o region in (E). ***$p < 0.001$; $n$
1013 = 5-8; One-way ANOVA with Tukey's multiple comparisons test.

1014 (G) Confocal Z projections of brains at 18 hr APF expressing GFP-αTub84B driven by
1015 TH-D'-Gal4 in control (top), AKT-CA (middle), and GSK3β-DN (bottom) groups. MB
1016 lobes labeled with anti-FasII.

1017 (H) Quantitation of GFP-αTub84B signal intensity in MP1o region in (G). **$p < 0.01$, ***$p$
1018 $< 0.001$; $n$ = 10-12; One-way ANOVA with Tukey's multiple comparisons test.